AD-A106 427 AIR FORCE INST OF TECH WRIGHT-PATTERSON AFB OH F/G 4/1
IONOSPHERIC DISTURBANCES DURING THE PERIOD 30 APRIL TO 5 MAY 19--ETC(U)
MAY 79 C D FRY
UNCLASSIFIED AFIT-CI-79-284T-S NL

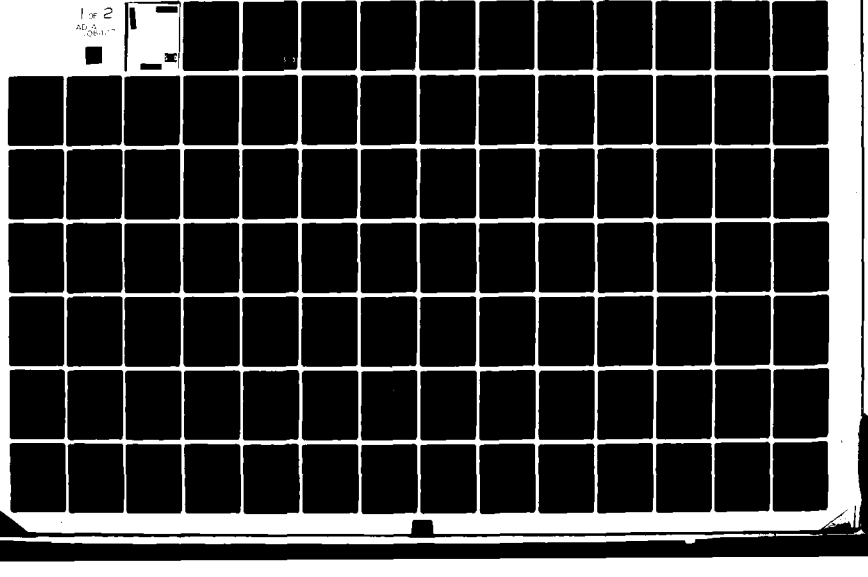

UNCLASS

SECURITY CLASSIFICATION OF THIS PAGE *(When Data Entered)*

REPORT DOCUMENTATION PAGE	READ INSTRUCTIONS BEFORE COMPLETING FORM
1. REPORT NUMBER: 79-284T-S	2. GOVT ACCESSION NO.: AD-A106427
3. RECIPIENT'S CATALOG NUMBER:	
4. TITLE *(and Subtitle)*: Ionospheric Disturbances During The Period 30 April to 5 May 1976	5. TYPE OF REPORT & PERIOD COVERED: THESIS/~~DISSERTATION~~
	6. PERFORMING ORG. REPORT NUMBER:
7. AUTHOR(s): Craig Daniel Fry	8. CONTRACT OR GRANT NUMBER(s):
9. PERFORMING ORGANIZATION NAME AND ADDRESS: AFIT STUDENT AT: Univ of Hawaii	10. PROGRAM ELEMENT, PROJECT, TASK AREA & WORK UNIT NUMBERS:
11. CONTROLLING OFFICE NAME AND ADDRESS: AFIT/NR WPAFB OH 45433	12. REPORT DATE: May 1979
	13. NUMBER OF PAGES: 103
14. MONITORING AGENCY NAME & ADDRESS *(if different from Controlling Office)*:	15. SECURITY CLASS. *(of this report)*: UNCLASS
	15a. DECLASSIFICATION/DOWNGRADING SCHEDULE:

16. DISTRIBUTION STATEMENT *(of this Report)*

APPROVED FOR PUBLIC RELEASE; DISTRIBUTION UNLIMITED

17. DISTRIBUTION STATEMENT *(of the abstract entered in Block 20, if different from Report)*

22 OCT 1981

FREDRIC C. LYNCH, Major, USAF
Director of Public Affairs
Air Force Institute of Technology (ATC)
Wright-Patterson AFB, OH 45433

18. SUPPLEMENTARY NOTES

APPROVED FOR PUBLIC RELEASE: IAW AFR 190-17

19. KEY WORDS *(Continue on reverse side if necessary and identify by block number)*

20. ABSTRACT *(Continue on reverse side if necessary and identify by block number)*

DD FORM 1 JAN 73 1473 EDITION OF 1 NOV 65 IS OBSOLETE

UNCLASS

SECURITY CLASSIFICATION OF THIS PAGE *(When Data Entered)*

IONOSPHERIC DISTURBANCES DURING THE PERIOD 30 APRIL TO 5 MAY 1976

by

Craig Daniel Fry

B.A., University of Hawaii, 1973

A thesis submitted to the Faculty of the Graduate School of the University of Colorado in partial fulfillment of the requirements for the degree of Master of Science

Department of Astro-Geophysics

1979

This thesis for the Master of Science Degree by

Craig Daniel Fry

has been approved for the

Department of

Astro-Geophysics

by

Sadami Matsushita

Sadami Matsushita

Kenneth Davies

Kenneth Davies

Theodore W. Speiser

Theodore W. Speiser

Date May 24, 1979

Fry, Craig Daniel (M.S., Astro-Geophysics)

Ionospheric Disturbances During the Period 30 April to 5 May 1976

Thesis directed by Professor Sadami Matsushita

Ionospheric behavior during solar disturbances and some theories of ionospheric storm mechanisms are reviewed. Variations in ionospheric parameters, fmin and foF2, from median values for May 1976 are analyzed using data from 72 ionospheric stations around the globe. Geomagnetic, auroral, interplanetary, and solar data are included in this analysis. A review is made of the solar-terrestrial events leading up to and during the 30 April to 5 May 1976 study period. The major solar flare on 30 April 1976 was followed by a typical enhancement of ionospheric D-region absorption in the sunlit hemisphere, but no appreciable change in foF2. An "ionospheric substorm" occurred over Europe following the 1200 UT 2 May 1976 geomagnetic substorm. The geomagnetic SSC at 1830 UT on 2 May 1976 was followed six hours later by a sharp ring current increase, a large geomagnetic substorm, and a sudden F-region disturbance on the dayside hemisphere. Peaks in foF2 appeared on the three storm days, 3-5 May 1976, over Japan at about 1-2 hours following local sunrise. Travelling ionospheric disturbances (TIDs) propagated toward the equator with

apparent horizontal velocities ranging from 718 to 368 $m\ sec^{-1}$, and periods averaging 2.5 hours. The sources of these TIDs probably lay in the northern-hemisphere auroral zone. Finally, the F-region variations are discussed in terms of theories of ionospheric storm mechanisms, including $\underline{E} \times \underline{B}$ drifts, thermospheric winds, and composition changes. Geomagnetic substorm time electric fields are suggested as a plausible source of ionospheric disturbances in middle and low latitudes.

This abstract is approved as to form and content.

Signed Sadami Matsushita
Faculty member in charge of thesis

Acknowledgements

I must first of all thank my good friend and teacher, Dr. S. Matsushita, who suggested the general topic of this thesis and guided me through all phases of this work to its completion. Many thanks to Dr. K. Davies and Dr. T. W. Speiser for the many informative discussions and critical reviews of the rough drafts of this thesis. I also appreciate the talks with Dr. A. Richmond concerning internal gravity waves. The ionospheric data was provided by World Data Center-A for Solar Terrestrial Physics, Boulder, Colorado, and the ionospheric forecasting branch of Air Force Global Weather Central, Offutt AFB, Nebraska. I am indebted to Irene Brophy for introducing me to ionograms, and to Irene and Doris Stansell for the data collection assistance at WDC-A. My 21-month stay at the University of Colorado was sponsored by the Air Force Institute of Technology Civilian Institutions Program. The University of Colorado supplied the computer time necessary for the data analysis, and the National Space Science Data Center, Greenbelt, Maryland, provided the solar wind data. I thank Richard and Deborah Guerra for the many hours of help with the art work on the figures, and assisting in the number crunching. Gail Maxwell offered sound advice on the format and typed the final copy of this thesis.

My deepest appreciation goes to my family for supporting me through it all. I am especially indebted to my wife, Susan, for typing the many rough drafts and supervising the art work. Without her assistance, support and patience, this thesis would never have been completed.

TABLE OF CONTENTS

PAGE

LIST OF TABLES

LIST OF FIGURES

FIGURE PAGE

FIGURE PAGE

FIGURE PAGE

CHAPTER 1

INTRODUCTION

The ionosphere has been defined by various authors as that part of the upper atmosphere which contains enough free electrons to affect the propagation of electromagnetic waves (see for example, Davies, 1965, p. 1; Rishbeth and Garriott, 1969, p. 3). The ionosphere has been divided into regions, which include: the D region from about 70 to 90 km altitude; the E region from about 90 to 150 km, and the F region above about 150 km. An ionospheric disturbance can be considered to be any deviation of ionospheric electron distribution from normal values. The disturbance is usually classified according to the method of observation, e.g., "short wave fade-out," or is discussed in terms of its morphology, such as a "sudden ionospheric disturbance" or "ionospheric storm." The ultimate cause of naturally occurring ionospheric disturbances is an input of solar energy into the ionospheric region, either directly by solar photon and particle radiation, or indirectly by an interaction of the solar wind with the magnetosphere, and then the ionosphere.

The purpose of this study is to investigate causes of ionospheric disturbances during the 30 April to 5 May 1976 period. This period of time was chosen for several reasons. First of all, it occurred at the statistical minimum of the 11-year solar activity cycle. The limited amount of solar activity provided the opportunity to study the terrestrial response to specific solar disturbance phenomena. Secondly, considerable amounts of data collection and analysis were accomplished during this period, because it had been selected in advance by the international scientific community as an interval of intense study.

In Chapter 2 ionospheric disturbances are discussed in terms of solar activity and, in a general way, the morphology of a typical storm is described. The ionospheric parameters used in this study and the method of analysis are explained in Chapter 3. A review of the events leading up to and during the study period are contained in Chapter 4. The data analysis and results are then presented. Particular emphasis is placed upon the immediate ionospheric response following the 30 April 1976 major solar flare, the F-region electron concentration behavior during the period 30 April to 5 May 1976, and travelling ionospheric disturbances during 2-3 May 1976. In Chapter 5 the results of this study are discussed in terms of theoretical models of ionospheric

storm mechanisms, and conclusions are drawn based on the results.

The ultimate goal of this thesis is to increase the understanding of the causes of ionospheric disturbances. This, in turn, will increase the reliability of forecasting disturbances and their impact on systems operating in the ionospheric environment.

CHAPTER 2

TYPICAL IONOSPHERIC DISTURBANCES

Ionospheric disturbances were perhaps first associated with geomagnetic storms by Hafstad and Tuve (1929), and by Appleton and Ingram (1935). It has long been known that geomagnetic activity was related to solar activity. Carrington reported that the first observed solar flare in 1859 was followed by a major geomagnetic storm (Carrington, 1859). It is now firmly established that ionospheric disturbances are directly associated with solar flares and indirectly with geomagnetic disturbances. Geomagnetic and ionospheric disturbances, in addition, have a tendency to recur at 27-day intervals in the absence of solar flares, even during solar sunspot minimum. Bartels (1932) postulated that geomagnetic activity of the recurring type resulted when the Earth came under the influence of mysterious areas, M-regions, tied to the sun's surface, sweeping by at 27-day intervals (Egeland et al., 1973, p. 16, 35). With the advent of observations from the space environment, the picture of solar-terrestrial interactions has become much clearer.

2.1 Solar Flares and Ionospheric Disturbances

The general features of solar flares can be summarized from observations following Svestka's (1976, p. 300-307) scheme. All flare production occurs in active solar regions with bipolar magnetic field structure. Small X-ray bright points can be seen within hours of the birth of the active region and sub-flares may occur within a day or so. Large flares usually occur after the development of sunspots and become most frequent as the active region develops to its maximum magnetic complexity. This is especially true of flares which produce impulsive X-ray bursts, interplanetary shock waves, and energetic protons (i.e., those most related to terrestrial disturbances). The flare is first seen in the chromosphere in H-alpha (6563 Å) light as a brightening along the neutral line of magnetic polarity reversals in existing plage areas. In proton-producing flares, the individual H-alpha bright points merge into ribbons paralleling the neutral line. The soft X-ray flux can be enhanced up to 10 minutes prior to the optical flare, but point brightenings of soft X-ray and EUV radiation are the first indications of a flare in progress. The flare X-ray and EUV spectra is thermal in nature, with a short non-thermal phase superimposed. The nonthermal phase of the flare starts after the soft X-ray enhancement onset and generally peaks

before the maximum H-alpha brightening. Hard X-ray, EUV, and microwave impulsive enhancements may take place during the non-thermal phase, perhaps due to some mechanism which accelerates electrons to high energies. The impulsive enhancements are attributed to bremsstrahlung radiation by these electrons. Travelling impulsive type III radio bursts (plasma waves excited by a stream of fast electrons with speeds averaging 0.3 c) are sometimes seen during the non-thermal phase and can be traced out to the distance of the Earth where an associated non-relativistic electron flux is observed in the near-Earth space. Type IV bursts, caused by electron gyro-synchrotron radiation, and type II bursts, assumed to be due to plasma oscillations caused by the passage of a shock wave through the coronal plasma, are sometimes observed with non-thermal flares. Any or all three of the radio burst types may be seen during a flare event, with the normal sequence being first type III, then type II, and then type IV radio bursts. The interpretation is that particles with energies up to 1 MeV are associated with type III bursts while much higher energy particles are generated by a process connected with type II and type IV bursts. A wave is sometimes seen to propagate at speeds of about 1000 km sec^{-1} across the chromospheric surface and is probably evidence of a fast MHD wave, which may develop into a shock wave generating the type

II burst. The shock may then travel to the Earth environment causing the sudden commencement of geomagnetic storms discussed below.

According to Svestka (1976), there is a high correlation between type II and type IV radio bursts and interplanetary shock waves and between type II bursts and energetic proton events. In general, flares which produce an intense energetic proton flux also produce interplanetary shock waves. When an interplanetary shock wave is produced by solar flare, the greatest portion of energy is carried in the shock (up to 5×10^{32} ergs) compared to the X-ray energy release of about 10^{30} ergs for a large flare. The longest lasting and most widespread of ionospheric disturbances, namely ionospheric storms, are also associated with the passage of the interplanetary shock wave past the Earth's bow shock.

High speed particle streams, formerly associated with M-regions, have recently been identified with coronal regions of open magnetic field structure or coronal holes (Krieger et al., 1973). According to Kopp and Holzer's (1976) model, high speed particle streams result when the divergence of the open field lines in coronal hole regions is rapid enough to produce supersonic flow low in the corona directed roughly radially outwards into the interplanetary medium. Interplanetary magnetic field structure is characterized by sectors of

predominantly one polarity, with magnetic field direction reversing at sector boundaries. The interplanetary magnetic field structure is probably quite complex, but the "sector structure" generally agrees with current space observations in the plane of the solar ecliptic. The high speed streams are most intense at the leading edge of a sector, immediately behind a sector boundary. High gradients in solar wind velocities at sector boundaries can account for tangential discontinuities, which are observed at shock fronts as they pass the Earth. Burlaga and Ogilvie (1969) determined that all intense sudden commencements of geomagnetic activity are caused by hydromagnetic shocks, whether associated with solar flares or with recurring phenomena. The interplanetary magnetic field polarity also plays in important role in geomagnetic and ionospheric variations as discussed below.

Ionospheric disturbances which occur simultaneously with the optical flare are generally referred to as "sudden ionospheric disturbances," or SID, and are usually classified according to the method used to observe them. It is now known that these SID's are caused by an enhanced ionization, particularly in the D region, due to increased X-ray and UV flux during a solar flare. Thus, only the sunlit hemisphere is affected immediately, but high energy protons may arrive soon after the photon flux and can have effects on D-region ionization in the

polar regions whether sunlit or not. It should be pointed out that rapid changes in ionospheric parameters during geomagnetic storms are often interpreted by some stations as SID's, even when no flares are observed.

Rishbeth and Garriott (1969, p. 190-192), Ratcliffe (1972, p. 91-92) and others, have summarized types of SID's which are described here according to the ionospheric region affected.

D-region electron content can increase by a factor of 10 or more during a major solar flare as the total X-ray emission rises by several orders of magnitude. Electron density increases suddenly, in a matter of several minutes, and slowly returns to normal values over a period of 3/4 to 1½ hours. High frequency (HF) radio waves which are usually reflected from the E and F regions may be absorbed by the enhanced D-region ionization. This "short wave fade-out," or SWF, can cause a total loss of signal over paths in the sunlit hemisphere. A sudden decrease in signal strength of HF galactic radio noise (observed at frequencies above the maximum ionospheric critical frequency), or "sudden cosmic noise absorption" (SCNA), is also seen as the D-region absorption increases. It should be pointed out that ionospheric radio wave reflection is actually due to continuous refraction of the electromagnetic wave as it travels through the ionospheric plasma (see, e.g., Davies, 1965).

Whereas medium and HF radio waves undergo enhanced absorption during SID's, very low frequency (VLF) wave D-region reflections are enhanced. An increase of VLF radio noise from distant electrical storms, or "sudden enhancement of atmospherics," or SEA, has long been used as an indicator of the occurrence of a flare. A sudden decrease in the height of VLF oblique reflection causes a "sudden phase anomaly," or SPA.

A magnetic "solar flare effect" (SFE) or "crochet" is observed as a change in the ground level geomagnetic field during a solar flare. The SFE has been attributed to increased electron density and conductivity at the level of the atmospheric dynamo current system (about 110 km), causing an increase in the normal daily solar variation of the geomagnetic field, Sq. During the 7 August 1972 solar flare the E-region ionization, as measured by the Millstone Hill incoherent scatter radar, increased by 100% at 125 km (Evans, 1973) and was accompanied by a large SFE with variations in the horizontal geomagnetic field component of 20-100 gammas (Mendillo et al., 1974).

A "sudden frequency deviation," or SFD, of stable HF signals such as WWV reflected from the E and F1 layers, is thought to be due to several effects (Donnelly, 1976). A decreased refractive index in the E region reduces the phase path (total transit time) of the radio wave. Also, the F1 layer reflection height is lowered

with increased ionization. Both effects can cause transient frequency changes on the order of several Hz for a 10 MHz signal (Rishbeth and Garriott, 1969, p. 192).

Increases in the maximum electron density of the F2 region, NmF2, have been observed during some flares (Knecht and Davies, 1961). More recently, sudden changes in the columnar integrated electron content have been identified with flares, and are called "sudden increases in total electron content," or SITEC. Evans (1973), Mendillo and Evans (1974), and Matsushita (1976) discuss a SITEC of 30% over preflare values based on the August 1972 Millstone Hill observations. They found the SITEC to be closely related to a sudden upward surge in the vertical electron drift over a range of 300 to 750 km.

High energy protons of roughly 1-10 MeV may arrive at the Earth several hours after a proton-producing flare and are directed along geomagnetic field lines to the polar cap ionosphere. Ionization produced by these energetic protons occurs between 50-90 km altitude and is primarily responsible for polar cap absorption (PCA) of HF radio waves. More energetic protons with energies on the order of 10^8 or 10^9 eV have been detected at the Earth's surface, with a latitudinal distribution dependent on particle energy. The arrival time of these "ground level events," or GLE, indicate the particle

trajectories can be quite complicated and need not arrive by a direct path along the interplanetary magnetic field lines connecting the flaring solar region with the Earth.

2.2 Ionospheric Storms

Ionospheric variations associated with geomagnetic storms are referred to as ionospheric storms. The most significant changes in the ionosphere during storms occur in the F region (Matuura, 1972). Parameters usually studied are maximum electron density in the F2 region, NmF2, total columnar electron content up to some altitude, N_T, and virtual height, h'F2. However, h'F2 is a measure of the delay time of a probing ionosonde signal, and changes in h'F2 are more of an indication of redistribution of electron density with height rather than actual height changes. The average height of F2 peak electron density, hmF2, usually varies less than 20 km during storms (Rishbeth, 1975). Therefore, NmF2 and N_T probably are better parameters to use when discussing storm variations of ionization. Other parameters which are studied include plasmasphere columnar electron content above some altitude (N_p), topside electron density above hmF2, and electron, ion, and neutral atmosphere temperature (T_e, T_i, and T_n). Sporadic E-layer ionization enhancements (E_s) and D-region electron content have also been studied during storm periods.

Geomagnetic storms appear to be related to changes in the solar wind parameters, either caused by solar disturbances, or changes of a recurring nature (Rishbeth and Garriott 1969, p. 253), which are now associated with coronal-holes as discussed previously. A typical storm may begin with a sharp increase in a geomagnetic field intensity at the ground in mid-latitudes on the order of tens of gammas, where 1 gamma = 10^{-9} Tesla = 1 nT. This sudden storm commencement, or SSC, results from the compression of the sunward magnetosphere by the impact of a travelling solar wind shock wave. A Forbush decrease in galactic cosmic ray intensity is sometimes observed and provides evidence of a shock wave passage. Satellite observations have shown the solar wind density and velocity to be enhanced behind the shock.

The enhanced solar wind plasma may continue to compress the magnetosphere and thus account for the initial phase increase of geomagnetic field intensity lasting for several hours.

A parameter often used to discuss the average variations of geomagnetic field measured at the Earth's surface is Dst, or storm time variation of magnetic field from non-storm values, and is determined by averaging geomagnetic horizontal field intensity around a low latitude band. The Dst calculation is an attempt to remove the non-storm diurnal changes in magnetic field

(Rishbeth and Garriott, 1969, p. 229), and is a measure of the ring current variations during storm periods.

A few hours after the SSC, the number of energetic particles mirroring in the magnetospheric trapping region increases. The energy and charge dependent drift of these trapped particles corresponds to an increase in the westward ring current which causes a decrease of about 100 gammas in magnetic field intensity at the Earth's surface (Ratclaffe, 1972, p. 95). Recovery of the geomagnetic field occurs slowly over several days as energetic ring current particles are lost by a variety of mechanisms. During the main and recovery phases of the typical geomagnetic storm, the polar geomagnetic field experiences shortlived disturbances, or polar substorms, a part of magnetospheric substorms. These substorm phenomena are thought to be due to currents flowing down along high latitude geomagnetic field lines, into the high latitude ionosphere, and back out along field lines. The probable generation mechanism of these field aligned currents is a magnetosphere dynamo associated with magnetic field line reconnections in the geomagnetic tail (Dungey, 1961; Speiser, 1976), and/or an instability mechanism such as the tearing mode instability (Shindler, 1974). Akasofu and Chapman (1972, p. 598) describe a geomagnetic storm as resulting from the frequent occurrence of intense substorms which inject hot plasma from

the magentospheric plasma sheet into the trapping region of the ring current.

Interplanetary magnetic field polarity, or IMFP, changes have been associated with geomagnetic and ionospheric disturbances. In particular, a change of IMFP from the northward (B_z) to the southward ($-B_z$) direction often precedes substorm occurrence. The direction of the IMG, toward or away from the sun, as well as the sign of B_z, appears to influence ionospheric current systems (Matsushita, 1975). B_z has been associated with F-region ionospheric drifts (Matsushita and Balsley, 1972; Rastogi and Chandra, 1974; Rastogi and Patel, 1975). However, Matsushita (1977) indicates that ionospheric disturbances are more likely caused by geomagnetic substorms or storms which are triggered by $-B_z$ instead of directly resulting from IMFP changes.

The ionospheric storm behavior depends upon latitude, season, storm stage, and other factors such as whether the geomagnetic storm is large or small. Statistical studies of large numbers of ionospehric storms, such as the one by Matsushita (1959), give the following general ionospheric behavior during geomagnetic storms. Worldwide variations of ionization distribution from normal values begin either at the time of a geomagnetic SSC or during the main phase of a geomagnetic storm. The ionospheric storm at higher latitudes is characterized by

an increase in NmF2 (the initial, or positive, phase) followed by a decrease below normal values (the main, or negative, phase), slowly returning to normal over a period of a few days (the recovery phase). At equatorial stations, the variations are statistically smaller and of the opposite sign of the high latitude variations. At lower mid-latitudes, summer and equinoctial storms have a behavior like the high latitude storms, while the winter behavior is like the equatorial storms.

Matuura (1972) reviewed ionospheric storms behavior and pointed out additional dependences. Very large geomagnetic storms are often accompanied by sharp decreases in NmF2 within an hour of SSC over a wide section of the globe, with no positive phase occurring. The largest decrease in NmF2 generally follows the largest Dst decrease by several hours. The plasmasphere columnar electron content decreases during increased geomagnetic activity and may take many days to return to prestorm values (Davies, 1978).

In addition to the storm time variations mentioned above, ionospheric storms have a strong local-time dependence. Storm NmF2 has smallest values shortly after sunrise and becomes largest in the evening (Martyn, 1953). Mendillo (1973) found the positive storm phase was most likely if SSC occurred between 0600 and 1500 LT. Matsushita (1959) showed that the change from positive

phase to negative phase begins first at high latitudes, moving to lower latitudes at an effective speed of about 50 to 150 m sec^{-1} (Davies, 1974).

The important mechanisms responsible for ionospheric storms include storm-time electric fields, thermospheric winds, and thermospheric composition and temperature changes (Matuura, 1972; Davies, 1974; Rishbeth, 1975; Paul et al., 1977).

Electrodynamic drifts due to the storm E fields can increase electron densities by transport of plasma into regions with lower ionization loss rates (Maturra, 1972), or can decrease electron densities by causing a loss of plasma to the plasmasphere (Park, 1971). Daytime eastward electric fields at the geomagnetic equator can produce an upward plasma drift at a velocity $\underline{E}\times\underline{B}/B^2$. The uplifted plasma then may diffuse down along magnetic field lines under the influence of gravity, and thus reduce the ionization at the equator (Martyn, 1947). This process has been referred to as the "fountain effect." Poleward electric fields at local sunset can create westward plasma drifts, resulting in enhanced ionization before sunset (Anderson, 1976).

Heating takes place in polar regions through Joule dissipation and collisional processes involving energetic precipitating particles. A pressure impulse due to the heating can set up thermospheric winds which propagate

to low latitudes (Richmond and Matsushita, 1975). In addition, $\underline{J} \times \underline{B}$ forces may be set up by the auroral electrojet current, and act to drive the winds. These winds affect ionospheric electron density by direct transport of plasma along magnetic field lines, or by altering the production and loss rates of ionization through the transport of composition and temperature changes (Matuura, 1972; Davies, 1974; Rishbeth, 1975). Wind shear can also create regions of enhanced ionization (Rishbeth, 1975). Heating in the auroral zone by processes mentioned above causes equatorward meridional winds. During the initially positive phase, plasma is transported up along magnetic field lines to regions of lower loss rate. However, neutral air enriched in molecular nitrogen and oxygen is also transported upwards and towards the equator. The modified atmospheric composition increases the ionization loss rate and the main negative phase begins. Recovery occurs over several days as the upper atmosphere returns to prestorm conditions through diffusion. Davies (1974) puts the heat source in the sunlit polar region. The influence of electric fields is ignored in this model, and should be considered when discussing actual storm behavior.

Oscillatory variations in ionospheric parameters during geomagnetic storms propagate over great distances, usually toward the equator. These travelling ionospheric

disturbances, or TID, are probably caused by internal gravity waves in the neutral atmosphere (Appendix A; Hines, 1960). Recent articles by Richmond (1978a, 1978b, 1978c) discuss the generation, propagation, and dissipation of gravity waves in a theoretical manner, and several excellent reviews on the subject of gravity waves and TID's exist in the literature (Yeh and Liu, 1974; Francis, 1975).

Although TID's have been identified with many sources, such as nuclear and volcanic explosions (Dieminger and Kohl, 1962; Davies and Baker, 1965; Loenard and Barnes, 1965), and thunderstorms (Davies and Jones, 1972), those seen during geomagnetic storms are caused by auroral disturbances. Gravity waves could be driven by a nearly horizontal Lorentz ($\underline{J}\times\underline{B}$) force perpendicular to the auroral electrojet and the main geomagnetic field. Alternatively, the waves could be launched by an atmospheric heat source such as Joule dissipation of heat or energetic particle precipitation in the same auroral regions. Richmond (1978a) showed that Joule dissipation is favored over other mechanisms acting in high latitudes to generate gravity waves. Chimonas (1970) showed that an equatorial electrojet Lorentz force or a pressure gradient driven by Joule heating were unlikely to create large amplitude gravity waves. However, he did not rule out Joule coupling as an equatorial TID

source during very large geomagnetic storms.

From theoretical considerations, large scale gravity waves can propagate at horizontal speeds of 300 to 1000 m sec^{-1}, with periods of 15 minutes to 6 hours, and horizontal wavelengths in excess of 1000 km (Francis, 1975; Richmond, 1979). In general, observed TID's fall in these ranges. Richmond (1978b) showed that the longer period and faster waves are least attenuated over large distances.

Stationary ionospheric disturbances are seen as simultaneous variations in ionospheric parameters at several stations. They may be linked to dawn-to-dusk magnetospheric electric fields (Park, 1971; Anderson, 1976) and interplanetary magnetic field changes (Matsushita, 1977).

The main goal of this thesis is to study ionospheric responses to disturbances of solar origin during the period 30 April to 5 May 1976. In particular, the immediate ionospheric response following the 30 April 1976 major solar flare, the F-region electron density variations during the study period, and travelling ionospheric disturbances on 2-3 May 1976, are investigated. Typical solar disturbance phenomena and their ionospheric responses have been reviewed in this chapter. In Chapter 3 the various ionospheric parameters used in this study are introduced, followed by a description of the procedure

used to analyze the data. Chapter 4 contains a discussion of the events leading up to, and during, the study period. An analysis of the data used in this investigation and results obtained are then presented. In Chapter 6 the results of this study are discussed in terms of theoretical models or at least theoretical ideas of ionospheric storm mechanisms, and conclusions are drawn based on the results.

CHAPTER 3

METHOD OF ANALYSIS

3.1 Ionospheric Parameters

The ionospheric response during the study period 30 April to 5 May 1976 is investigated in terms of the variation of several ionospheric parameters. These parameters will be defined in this chapter and their method of observation will be described. Finally, the procedure used to analyze the available data for these parameters will be discussed.

As discussed in Chapter 2, the various regions of the ionosphere respond differently to disturbance sources. The D-region ionization (between about 70 and 90 km) may be increased by a factor of ten during a large solar flare, while the F region (above about 150 km) is much less affected. However, during geomagnetic storms, the mid-latitude ionospheric electron concentration varies mainly in the F region. Similarly, travelling ionospheric disturbances are primarily an F-region phenomena.

Many methods have been used to study ionospheric parameters including vertical incident ionospheric sounders, incoherent (Thompson) scatter radar, satellite borne topside sounders, and in situ plasma probes. The

ground-based ionospheric sounder, or ionosonde, has been around the longest, and is the most widespread system in use. An ionosonde produces an "ionogram" photographically, or more recently, digitally, which shows the variation of the apparent height of reflection of a transmitted radio pulse as a function of frequency. The apparent or virtual height of reflection, h', in a plane-stratified plasma can be determined from the time delay between transmission and display of the radar pulse on the ionogram. The group velocity of the incident wave is retarded travelling through the plasma, so the virtual height is always greater than the actual height of reflection. As the ionosonde signal is swept to higher frequencies, the radio wave is increasingly retarded to the point that the slope of h' becomes infinite. This "critical frequency" is related to the maximum electron density at the layer of reflection. An idealized ionogram has been sketched in Figure 1, showing the parameters discussed here. Actual ionograms vary greatly in appearance depending upon such factors as equipment, location, local time, season, etc. Figure 2 is traced from actual ionograms taken at Mexico City and Boulder.

The geomagnetic field allows several modes of propagation in the ionospheric plasma. A radio wave incident upon the ionosphere is divided into two magnetic-electronic component waves, the ordinary and

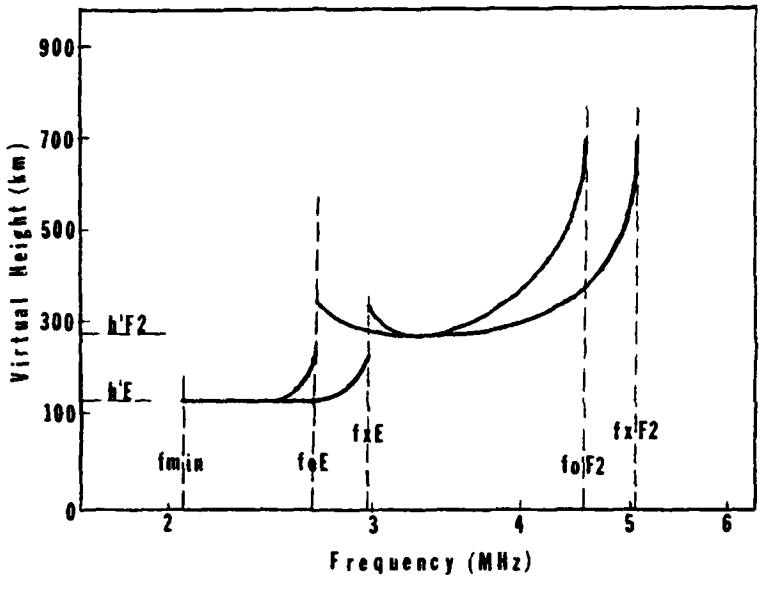

FIGURE 1 Idealized ionogram with two ionospheric layers, E and F2, present. Virtual heights (h'E, h'F2), minimum observed trace frequency (fmin), and critical frequencies (foE, fxE, foF2, fxF2) are shown.

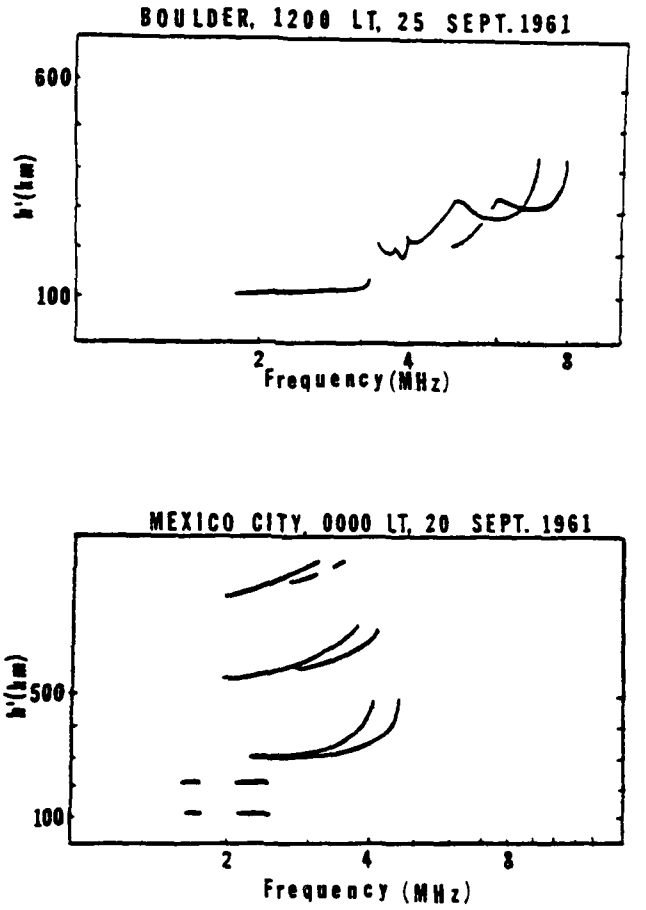

FIGURE 2 Ionogram traces from Boulder, Colorado (lat. 48.9°N, long. 316.4° geomagnetic) at 1900 UT (local noon) 25 September 1961, and Mexico City, Mexico (lat. 29.1°N, long. 326.8° geomagnetic) at 1600 UT (local midnight) 20 September 1961. Diagrams were traced from ionograms in UAG-10 (p. 11 A-69, II B-41, 1970).

extraordinary modes, which propagate independently in the plasma. The Appleton equation in a collisionless plasma is

$$n^2 = 1 - \frac{2X(1-X)}{2(1-X) - Y_T^2 \pm \left[Y_T^4 + 4(1-X)^2 Y_L^2\right]^{\frac{1}{2}}} \quad , \quad (3.1)$$

where n is the refractive index, X = (plasma frequency/wave frequency)^2, $Y_T = Y\sin\theta$, $Y_L = Y\cos\theta$, Y = electron gyrofrequency/wave frequency, and θ is the angle between the wave normal and the geomagnetic field (Davies, 1965, p. 71).

This equation can be solved for the condition of reflection, n = 0, to yield the frequencies of reflection for the two modes. The ordinary wave is reflected at the point where the plasma frequency equals the wave frequency, i.e., X = 1. Thus, the ordinary wave reflection does not depend upon the background geomagnetic field. The extraordinary wave is reflected at the level where X = 1-Y for wave frequencies above the gyrofrequency, and at X = 1+Y below the gyrofrequency. The extraordinary mode does depend upon the background magnetic field. For this reason, the ordinary mode ionogram trace is generally used to study ionospheric plasma density.

The maximum electron density, Nm at the reflection point is related to the ordinary mode critical frequency fo, by

$$Nm = 1.24 \times 10^{10} \, fo^2 \quad , \qquad (3.2)$$

where Nm is in units of meters^{-3} and fo is in megahertz. The F2-layer maximum electron density is thus proportional to the square of the critical frequency at this level, foF2, and it is foF2 which is used to study the F-region storm behavior in this paper.

The lowest frequency at which the transmitted radio pulse is reflected, regardless of mode of propagation, is called "fmin," and is roughly a function of absorption in the lowest ionospheric region (the D region during the day; Davies, 1965, p. 133). This parameter is useful to study enhanced absorption of HF radio waves due to solar-flare X-rays, or due to particle precipitation in high latitudes.

In general, ionograms are obtained in 15-minute intervals, or at least on each hour at over 100 stations around the world. A reading accuracy of 0.1 MHz is usually obtainable for both fmin and foF2. Copies of ionograms and tabulations of hourly parameters, including fmin and foF2, are archived at several regional World Data Centers. For an in-depth study of ionogram analysis, the reader is referred to reports UAG-10 (1970) and UAG-23 (1972; 1978) from the World Data Center.

Columnar electron content, often referred to as total electron content, or TEC, is the line integrated

electron concentration along the ray path from a transmitted (or reflected) radio signal to a receiver. VHF radio beacons on geostationary staellites are commonly monitores to obtain TEC. The Faraday rotation method of determining TEC actually approximates the columnar electron content from the receiver out to some altitude, usually around 2000 km. The rotation angle of a linearly polarized wave vector, Ωf, is approximately proportional to the columnar electron content. Other methods determine the actual TEC along the ray path. These methods make use of the dependence of the phase difference, at the receiver, of two transmitted waves at different frequencies upon the integrated electron density along the path. By taking the difference of Faraday electron content, Nf, and actual TEC, or Nt, the plasmaspheric content (above about 2000 km) can be determined and studied continuously during storms (Davies, 1978). Other methods of studying plasmaspheric electron content such as using whistler data were not investigated in this study.

3.2 Procedure

Hourly foF2 data from 72 ionospheric stations were obtained for the period 30 April to 5 May 1976. Tabulated data were provided by World Data Center A, Upper Atmosphere Geophysics, Boulder, Colorado (WDC-A), and Air Force Global Weather Central, Offutt AFB, Nebraska. Ionograms and f-plots (ionogram summaries in a frequency versus time format) from WDC-A were used to obtain 15-minute values of foF2 from 2 to 5 May 1976 for 20 stations. Also, foF2 and fmin from 1800 UT 30 April to 0200 UT 1 May 1976 were obtained for 6 stations. Monthly median foF2 and fmin were either provided by WDC-A or calculated by the author.

Median values of an hourly parameter are calculated by first ordering the values during each day of a month at each local time in ascending order of value. The middle value (for an odd number of values) or the average of the two middle values (for an even number of values) is then the monthly median at that local time.

The deviations of foF2 and fmin from the monthly medians, ΔfoF2 and Δfmin, were then calculated for the entire data set. For example, the deviation of hourly foF2 from the monthly median is determined from the relationship

$$\Delta foF2_i = foF2_i - \overline{foF2_i} \quad (MHz) , \qquad (3.3)$$

where $foF2_i$ is the value of foF2 measured by an ionospheric station at time i, and $\overline{foF2_i}$ is the monthly median value at this same time. Fifteen-minute values of ΔfoF2 were also obtained by first linearly interpolating the hourly monthly medians and then following the procedure above. A similar relation was used to determing the deviation of fmin.

This method is commonly used in an attempt to remove non-storm diurnal variations from the data set (see Matsushita, 1959). It should be pointed out that the median is not an average and may not correspond to the actual quiet (non-storm) ionospheric behavior. However, the parameter is widely used, and does allow the general diurnal behavior to be approximated.

From Equation (3.1), it can be seen that deviations of maximum F-region electron concentration, ΔNmF2 is linearly related to ΔfoF2 by

$$\Delta NmF2 \approx 2\Delta foF2 \quad . \tag{3.4}$$

Finally, hourly and 15-minute foF2 data for all 72 stations were plotted in several formats to facilitate the analysis of the ionospheric storm time variations.

CHAPTER 4

IONOSPHERIC AND THERMOSPHERIC RESPONSE DURING THE DISTURBANCE PERIOD

4.1 Background

The disturbance period from 30 April to 5 May 1976 is of particular interest to the study of solar-terrestrial interactions because it occurred near the statistical minimum of the 11-year solar activity cycle. The major solar flare on 30 April and subsequent geomagnetic and ionospheric disturbances provide scientists with the opportunity to study relatively isolated disturbance events. In this way a better understanding of terrestrial and interplanetary responses to specific solar phenomena may be obtained.

The inverval of 15 March to 15 May 1976 had been selected in advance for special study by the Study of Travelling Interplanetary Phenomena (STIP) project of the Special Committee on Solar-Terrestrial Physics (SCOSTEP). This was primarily due to the opportune positions of several spacecraft during this period. The sun reached a high level of activity intermittently during late March through early May. The Monitoring Sun-Earth Environment (MONSEE) committee of SCOSTEP selected 20

March to 5 May 1976 to be a Retrospective World Interval of special study (Shea, 1977). Therefore, considerable data collection and analysis were accomplished for the period of interest in this paper.

In this chapter a brief discussion of the enhanced solar activity during March to May 1976 is presented, followed by a more detailed analysis of terrestrial ionospheric responses to the solar events of 30 April 1976. Particular emphasis is placed on the F-region behavior during the geomagnetic storm of 2-5 May 1976. Finally, travelling ionospheric disturbances (TID) are studied and attempts are made to determine TID velocities and source regions.

4.2 Solar-Terrestrial Disturbance History

Various phenomena associated with the March to May 1976 solar-terrestrial disturbance period have been presented in the WDC-A Report UAG-61 (1977) and AFGL Special Report No. 209 (1977).

Solar activity declined towards sunspot minimum during late 1975 and early 1976. Monthly averaged sunspot numbers during December 1975 through February 1976 remained below 10. Solar activity increased abruptly in March 1976 with the appearance of flare-producing McMath Plage regions 14127 and 14143 (SGD, 1976). (The McMath identification scheme is used to number solar active

regions, based upon the occurrence of plages, or bright areas when viewed in H-alpha light indicating an area of activity.) Plage 14127 (latitude N05, Carrington longitude about 196°) generated 12 flares accompanied by SWFs on its transit across the solar disk in March, but had diminished in size and activity by the time it re-appeared on the east limb at Plage 14161. Another minor active region, McMath Plage 14168 (N06, Carrington longitude about 130°), produced some minor flare activity with Type II and Type IV radio bursts on 20 April. However, the major source of terrestrial disturbances during this entire period was Plage 14143/14179 (S07, Carrington longitude about 44°). This region first appeared as McMath Plage 14118 in early March, but rotated over the west limb without much activity. Upon its return on the east limb, the region was renumbered 14143 and had grown to be a very magnetically complex region (Dodson and Hedeman, 1977). SIDs were associated with major flares on 25, 28, and 31 March. In all, 13 flares from Plage 14143 produced SWFs on this transit of the disk.

Subflares from this region on 23 March were followed by a geomagnetic SSC at 0233 UT on 26 March with the Ap index reaching 138 on that day. (Ap is a daily averaged geomagnetic activity index on a linear scale of 0 to 400 with 400 corresponding to the most disturbed periods.) A parallel ribbon flare of importance 1n and associated

with X-ray and Type IV radio bursts began at 1138 UT on 31 March, followed by an SSC at 0255 UT on 1 April (Shea, 1977).

Plage 14143 passed over the west limb on 6 April and returned as Plage 14179 on 20 April, considerably reduced in size and complexity. However, by 28 April, the region has again grown in magnetic complexity and subflare activity took place throughout 28 April to 1 May (SGD, 1976). A major solar flare began at about 2047 UT on 30 April (as observed in H-alpha light), followed by terrestrial disturbances during the next 5 days. This flare will be discussed in more detail below.

The geomagnetic field during March to May exhibited periods of quite enhanced activity and also periods of very low levels of activity. Figures 3-6 show the behavior of the daily sunspot number, the solar wind bulk speed as measured by the IMP 7 and 8 spacecraft, and the geomagnetic Ap and equatorial Dst indices (SGD, 1976; Dodson and Hedeman, 1977). Major flares and SSCs are also indicated in Figure 6. The 27-day recurrence pattern of geomagnetic activity is evident. It roughly corresponds to variations in the solar wind bulk speed, with enhancements in geomagnetic activity due to flare generated shock waves superimposed.

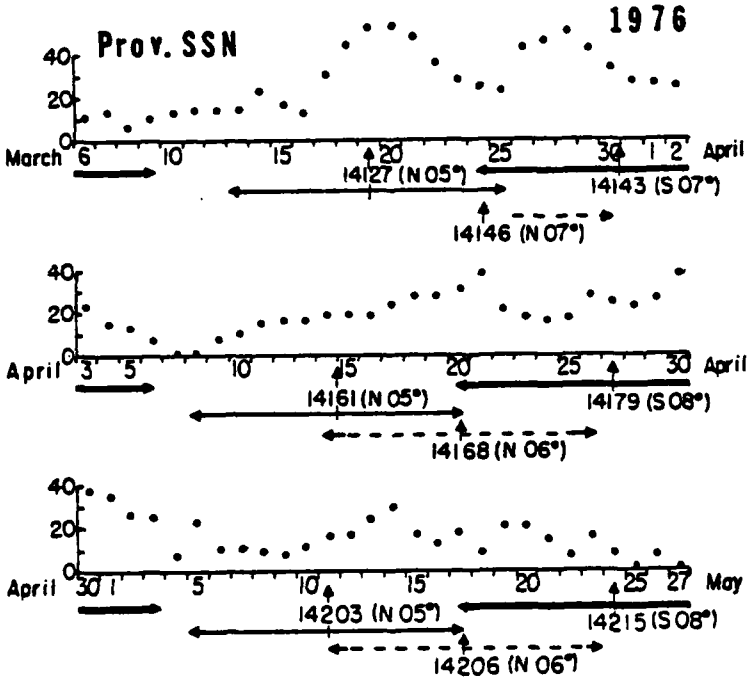

FIGURE 3 Provsional daily averaged sunspot number for March to May 1976 showing McMath Plage regions. Central meridian passage of each region is indicated by vertical arrows (from Dodson and Hedeman, 1977).

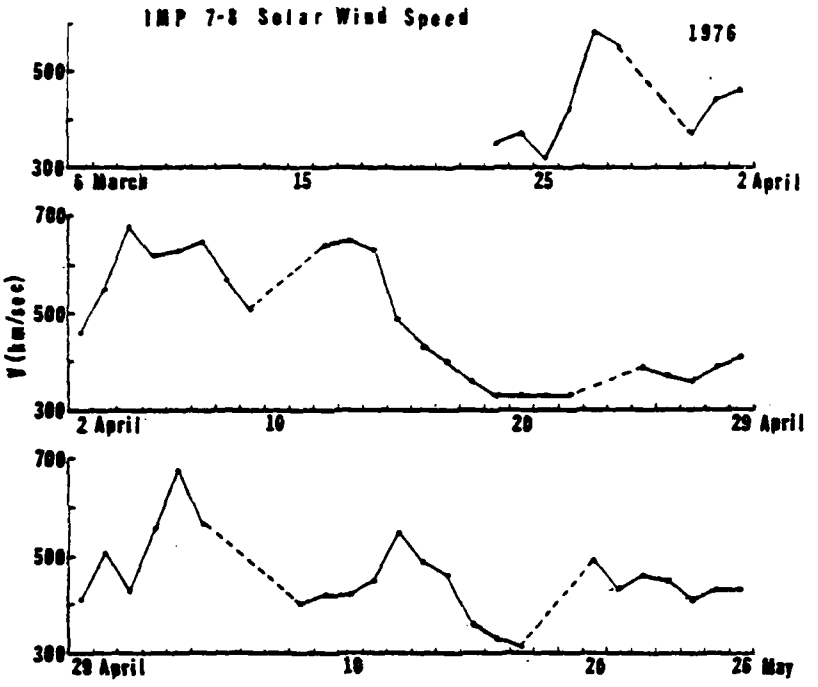

FIGURE 4 Daily averaged solar wind speed from IMP 7 and 8, March to May 1976. Missing data are indicated by dashed lines.

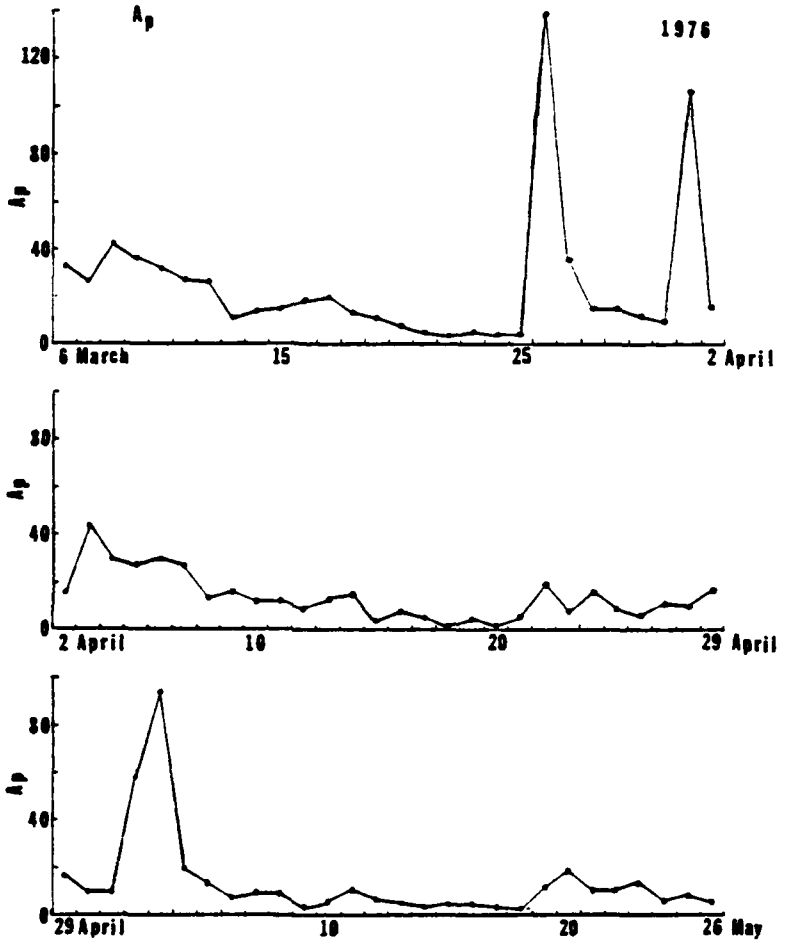

FIGURE 5 Ap for March to May 1976. This period corresponds to Bartel's solar rotation numbers 1950 to 1952 (SGD, 1976).

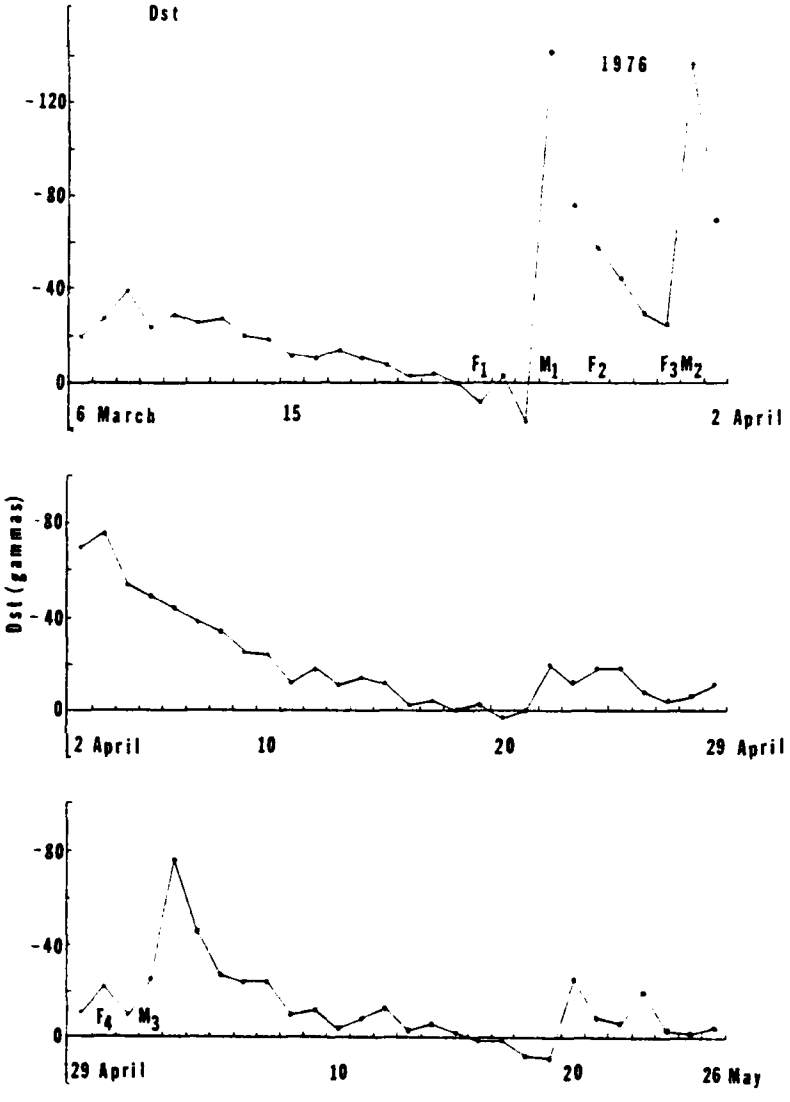

FIGURE 6 Daily averaged Dst for March to May 1976. This period corresponds to Bartel's solar rotation numbers 1950 to 1952. Major solar flares are indicated by F_1-F_4, and storm sudden commencements by M_1-M_3 (SGD, 1976).

4.3 Flare-Coincident Ionospheric Disturbances

The first indication of the 30 April 1976 major flare was an enhancement of the 1-8 Å X-ray channel on geostationary satellite GOES-1, at 2043 UT (Figure 7). The optical flare began with an H-alpha brightening in McMath Plage 14179 (S09, W46) at 2047 UT simultaneous with the onset of a 2800 MHz solar radio noise burst measured at Ottawa (Shea, 1977). This radio burst and the H-alpha flare brightening peaked at about 2109 UT, followed by the X-ray enhancement peak at 2114 UT in both the 1-8 Å and the 0.5-4 Å bands. A Type IV radio burst was recorded at Sagamore Hill, Massachusetts, and at the Harvard Radio Astronomy Station, Fort Davis, Texas, from 2103 to 2130 UT (Castelli et al., 1977; Maxwell 1977).

A Type III radio burst began at 2108 UT as observed by Harvard, followed by Type II emission from 2107 to 2130 UT. Maxwell (1977) suggests this flare was accompanied by a piston-driven shock wave, and indeed, a geomagnetic SSC occurred approximately 46 hours after the flare onset (Figure 6).

The immediate ionospheric response was quite pronounced on the sunlit hemisphere. Figure 8 shows the sunlit portion of the globe at 2100 UT on 30 April 1976. A sudden increase in total electron content of about 10% was measured at Havana, Cuba, between 2047 and 2235 UT, as shown in Figure 9 (Jakawski and Lazo, 1977).

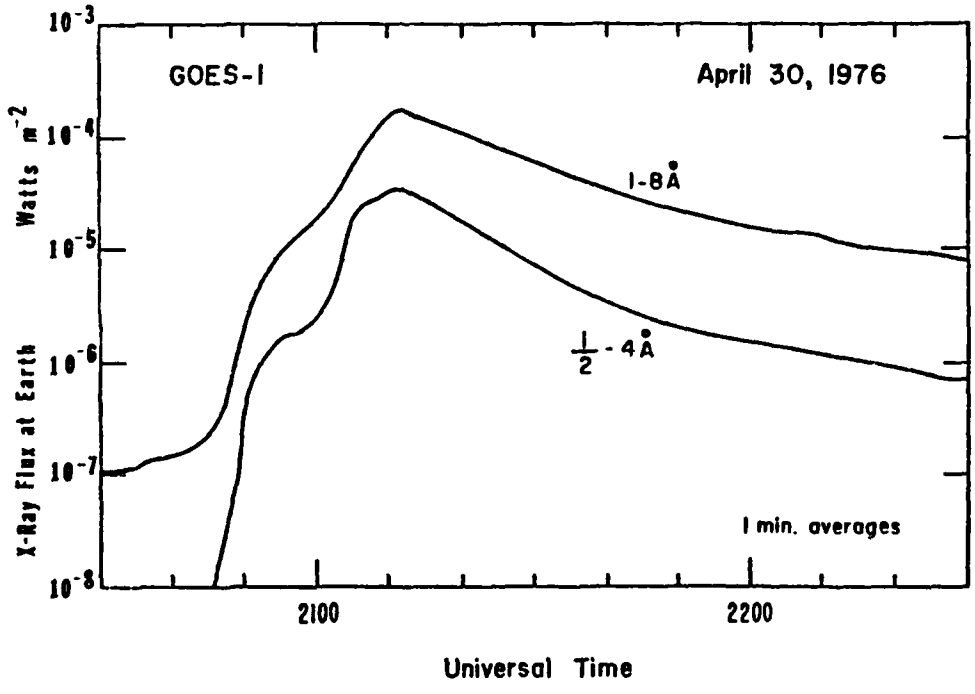

FIGURE 7 GOES-1 X-ray data for 30 April 1976. The 1-8 Å and 0.5-4 Å channels are displayed. X-ray enhancement onset was at 2043 UT with peak flux at 2114 UT (SGD, 1976).

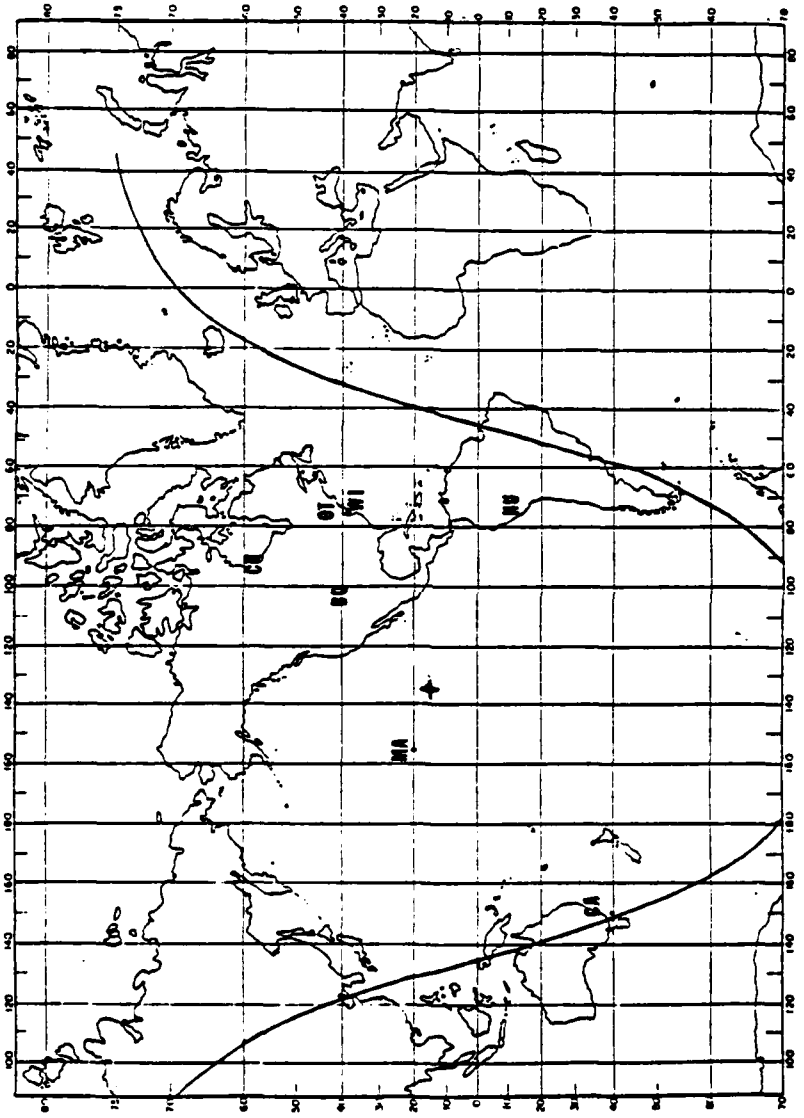

FIGURE 8 Sunlit portion of the Earth's surface at 2100 UT on 30 April 1976. The subsolar point is indicated by the circle-plus symbol at about $15^{o}N$ latitude, $135^{o}W$ longitude, geographic

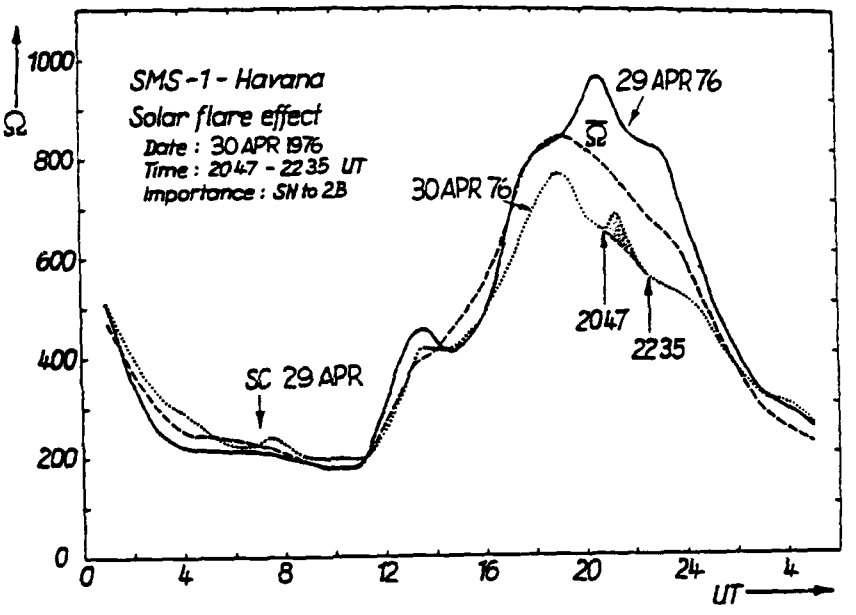

FIGURE 9 Relative Faraday polarization angle, Ω, proportional to columnar electron content, at Havana, Cuba. The mean variation for 24-29 April 1976 (dashed line) is compared with the variation for 29 April (solid line) and 30 April (dotted line) 1976. The solar flare effect from 2047 to 2235 UT on 30 April 1976 is indicated (Jakowski and Lazo, 1977).

Ichinose and Ogawa (1977) reported a sudden frequency deviation (SFD) on the sunlit path of a 5 MHz signal received at Kyoto, Japan. The SFD reached a peak positive value of 0.3 Hz at 2103.5 UT and peak negative value at 2104.9 UT. A comparison of the Maui 15-minute foF2 and fmin with SMS-2, 0.5-4 Å, and 1-8 Å X-ray flux is shown in Figure 10 for 1800 UT 30 April to 0200 UT 1 May. Radio absorption and X-ray flux reach their peaks at about the same time, as would be expected, and foF2 exhibits no obvious deviations from the roughly linear increase with time as it climbs towards the afternoon maximum.

Deviations of 15-minute values of fmin and foF2 from April monthly median values are presented in Figure 11 for 1800 to 2343 UT on 30 April for the stations Huancayo, Wallops Island, Ottawa, and Churchill. The locations of these stations and the others used in this study are given in Table 1. Total loss of ionosonde returned signal (blackout) occurred between 2115 and 2130 UT at Wallops Island and at 2115 UT at Churchill. Enhancements in Δfmin reached 4 MHz at Huancayo and 3 MHz at Ottawa. Delta foF2 values were less than ±1 MHz at the three low-latitude stations and no obvious increases or decreases were associated with the solar flare. Hourly Δfmin values were obtained for several other stations (Townsville, Mundaring, Halley Bay, Christchurch, Campbell Island, and

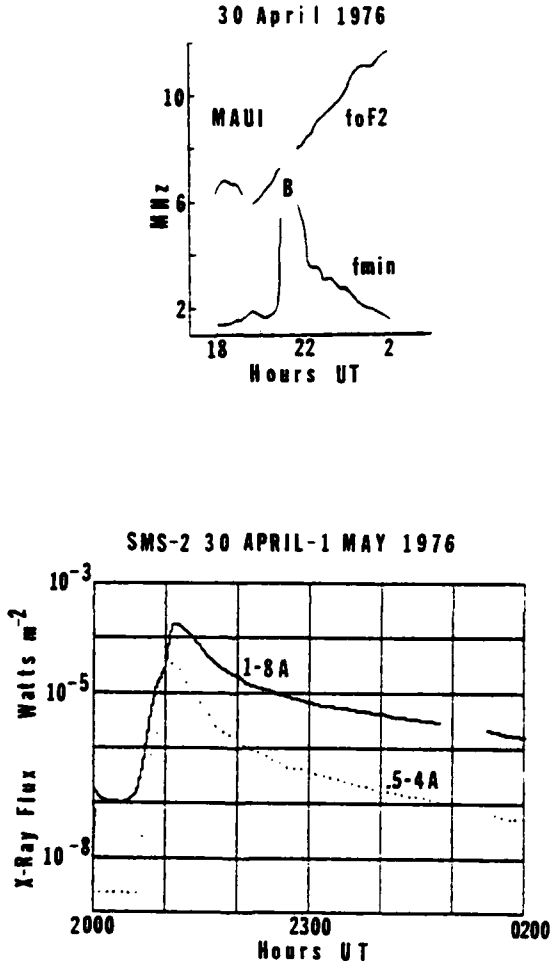

FIGURE 10 Fifteen-minute values of foF2 and fmin at Maui, Hawaii (top diagram) are displayed with SMS-2 1-8 Å and 0.5-4 Å X-ray data (bottom diagram) for 30 April to 1 May 1976. Total absorption of the ionosonde signal is indicated by B.

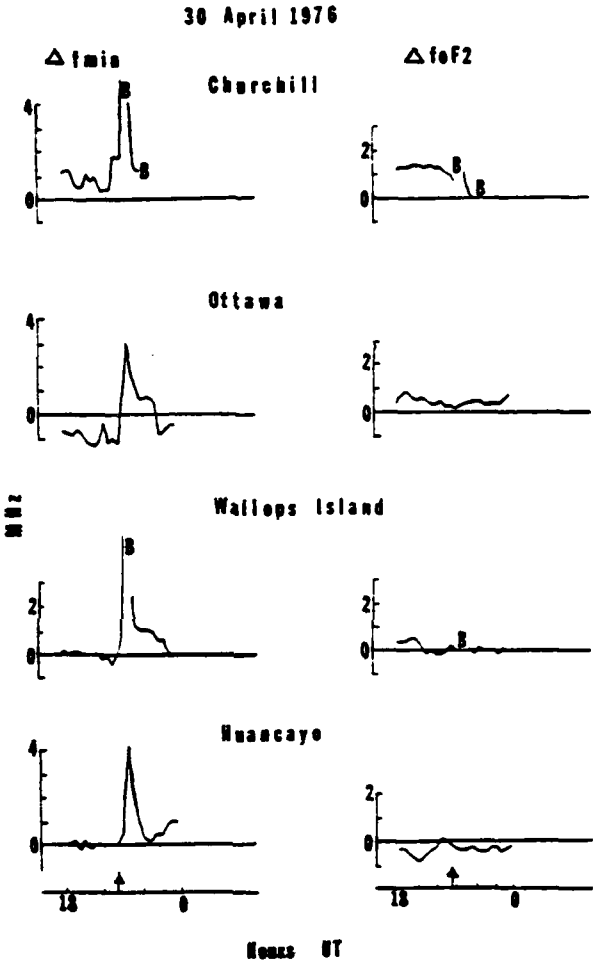

FIGURE 11 Deviations of 15-minute values of fmin and foF2 from April monthly median values are presented for Churchill, Ottawa, Wallops Island, and Huancayo. The X-ray solar flare onset at 2043 UT on 30 April 1976 is shown by arrows. Total absorption of the ionosonde signal is indicated by B.

TABLE I

LIST OF IONOSPHERIC STATIONS BY GEOMAGNETIC LATITUDE

Station	Symbol	Geographic Lat.	Geographic Long.	Geomagnetic Lat.	Geomagnetic Long.	ΔUT
THULE	TH	76.4N	68.3W	89.7N	1.0	-5
RESOLUTE BAY	RE	74.7N	94.9W	83.0N	289.3	-6
GODHAVN	GO	69.3N	53.5W	79.8N	32.5	-3
NARSSARSSUAQ	NA	61.2N	45.4W	71.2N	36.8	-3
CHURCHILL	CH	58.8N	94.2W	68.7N	322.6	-6
KIRUNA	KI	67.8N	20.4E	65.3N	115.5	1
COLLEGE	CO	64.9N	147.8W	64.7N	256.5	-10
GOOSE BAY	GB	53.3N	67.8W	64.6N	12.1	-5
SODANKYLA	SO	67.4N	26.7E	63.8N	120.0	2
LYCKSELE	LY	64.6N	18.7E	62.8N	111.0	1
WINNIPEG	WN	49.9N	97.4W	59.6N	322.7	-6
ST. JOHNS	SJ	47.6N	52.7W	58.5N	21.2	-4
UPSALLA	UP	59.8N	17.6E	58.5N	105.9	1
NURMINJARVI	NU	60.5N	24.7E	57.9N	112.5	0
SALEKHARD	SA	66.5N	66.5E	57.3N	148.9	4
OTTAWA	OT	45.4N	75.9W	56.8N	351.1	-5
LENINGRAD	LE	60.0N	30.7E	56.3N	117.4	2
JULIUSRUH/RUGEN	JR	55.0N	13.4E	54.5N	98.7	1
SLOUGH	SL	51.5N	.6W	54.3N	84.1	0
DE BILT	DE	52.1N	5.2E	53.8N	89.4	1
LINDAU	LI	51.7N	10.1E	52.3N	93.9	1
DOURBES	DO	50.1N	4.6E	52.0N	87.7	0
MOSCOW	MO	55.5N	37.3E	50.9N	120.5	2
YAKUTSK	YK	62.0N	129.7E	50.9N	193.7	9
MAGADAN	MG	60.1N	151.0E	50.8N	210.8	10
GORKY	GK	56.2N	44.3E	50.3N	126.7	3
PRUHONICE	PR	50.0N	14.6E	49.9N	97.4	0
POITIERS	PT	46.6N	.3E	49.5N	81.8	0
WALLOPS ISLAND	WI	37.9N	75.5W	49.2N	348 5	-5
BOULDER	BO	40.0N	105.3W	48.9N	318.4	-7
SVERDLOVSK	SV	56.7N	61.1E	48.5N	140.7	4
FRIEBURG	FR	48.1N	7.6E	48.4N	90.0	0
GRAZ	GR	47.1N	15.5E	47.0N	96.9	1
TOMSK	TO	56.5N	84.9E	45.9N	159.6	6
TORTOSA	TT	40.8N	.5E	43.9N	79.5	0
ROSTOV	RO	47.2N	39.7E	42.5N	119.2	3
VANDENBERG AFB	VB	35.0N	121.0W	41.0N	303.0	-8
PATRICK AFB	PA	28.2N	80.6W	39.4N	347.3	-5
KHABOROVSK	KH	48.5N	135.1E	37.9N	200.4	9
TBILISI	TB	41.7N	44.8E	36.2N	122.5	3
WAKKANAI	WK	45.4N	141.7E	35.3N	208.0	9
ALMA ATA	AA	43.3N	75.9E	33.4N	150.7	5
ASHKHABAD	AS	37.9N	58.3E	30.4N	132.3	4
AKITA	AK	39.7N	140.1E	29.5N	205.4	9
MEXICO CITY	ME	19.3N	99.6W	29.1N	326.8	-6
KOKUBUNJI	KO	35.7N	139.5E	25.4N	205.4	9
MAUI	MA	20.8N	156.5W	20.9N	268.1	-10
YAMAGAWA	YA	31.2N	130.6E	20.3N	197.8	9
DELHI	DL	28.6N	77.2E	18.9N	148.9	5
AHMEDABAD	AH	23.0N	72.6E	13.8N	148.9	5
TAIPEI	TP	25.0N	121.5E	13.7N	189.8	8
BOMBAY	BM	19.0N	72.8E	9.8N	143.6	5
MANILA	MN	16.4N	120.6E	5.1N	189.2	8
TIRUCHIRAPALLI	TI	10.8N	78.7E	1.0N	148.3	5
KODAIKANAL	KK	10.2N	77.5E	.6N	147.1	5
HUANCAYO	HU	12.1S	75.3W	.6S	358.8	-5
RARATONGA	RA	21.2S	159.8W	20.9S	273.6	-11
BUENOS AIRES	BA	34.6S	58.5W	23.2S	9.4	-4
JOHANNESBURG	JO	26.1S	28.1E	26.9S	91.3	2
TOWNSVILLE	TV	19.3S	146.7E	28.5S	218.8	10
HERMANUS	HM	34.1S	18.3E	32.8S	79.7	2
BRISBANE	BR	27.5S	152.9E	35.7S	226.9	10
PORT STANLEY	PS	51.7S	57.9W	40.4S	9.1	-4
MUNDARING	MD	32.0S	116.2E	43.5S	186.1	8
CANBERRA	CA	35.3S	149.2E	44.0S	224 3	10
CHRISTCHURCH	CR	43.6S	172.8E	48.1S	252.8	12
HOBART	HO	42.9S	147.3E	51.7S	224.3	10
ARGENTINE ISLAND	AR	65.3S	64.3W	53.8S	3.3	-4
CAMPBELL ISLAND	CI	52.6S	169.2E	57.3S	253.2	11
HALLEY BAY	HB	75.5S	26.7W	65.8S	24.3	-2
SYOWA BASE	SY	69.0S	39.6E	69.7S	77.7	3
SCOTT BASE	SB	77.9S	166.8E	79.0S	294.2	11

Canberra), near the terminator and no flare-associated enhancements were noticed.

Hourly foF2 and fmin for 30 April 1976 at Maui, Hawaii, are shown in Figure 12. The local time variation of maximum F2 electron density followed the usual diurnal variation while hourly fmin was suddenly enhanced between 1000 and 1100 local time (2000-2100 UT) to greater than 5 MHz with total balckout of the reflected vertical incident signal at 2115 and 2130 UT. The enhanced D-region absorption remained above 2 MHz for approximately 5 hours at Maui,

A geomagnetic flare effect (SFE) was reported at Huancayo between 2102 and 2130 UT (SGD, 1976). The SFE at Boulder (Figure 13) can be seen in the geomagnetic field H, Z, and D components. Horizontal field intensity decreased by about 12 gammas, with declination changing by 5 minutes of arc to the west. These changes can be explained by an increase in the Sq current over Boulder due to increased conductivity at the altitude of the current system as a result of enhanced ionization during the flare. The enhanced absorption in the sunlit hemisphere, the Havana sudden increase in TEC, and the general lack of F-region response also demonstrate that the flare-associated electron density increase occurred primarily in the lower ionospheric regions.

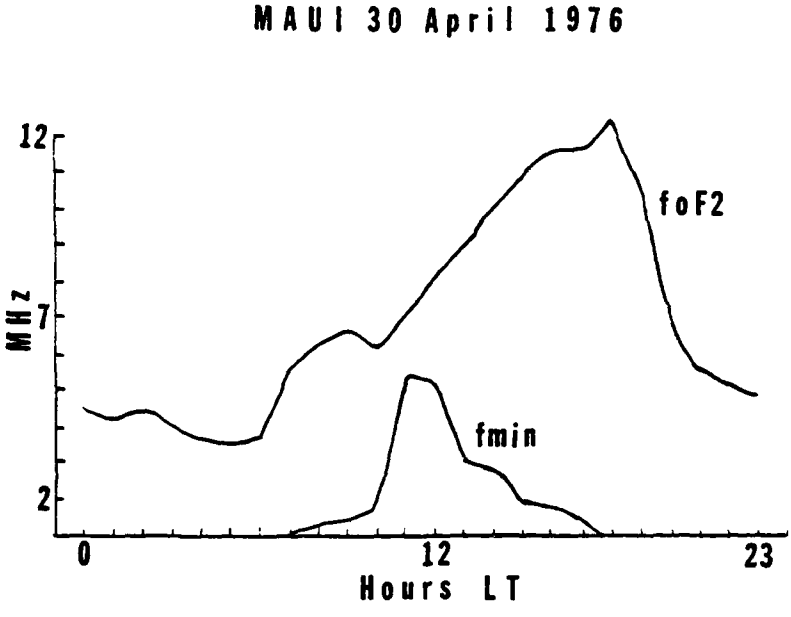

FIGURE 12 Maui, Hawaii, hourly foF2 and fmin data for 0000 to 2300 local time 30 April 1976 (1000 UT 30 April to 0900 UT 1 May 1976).

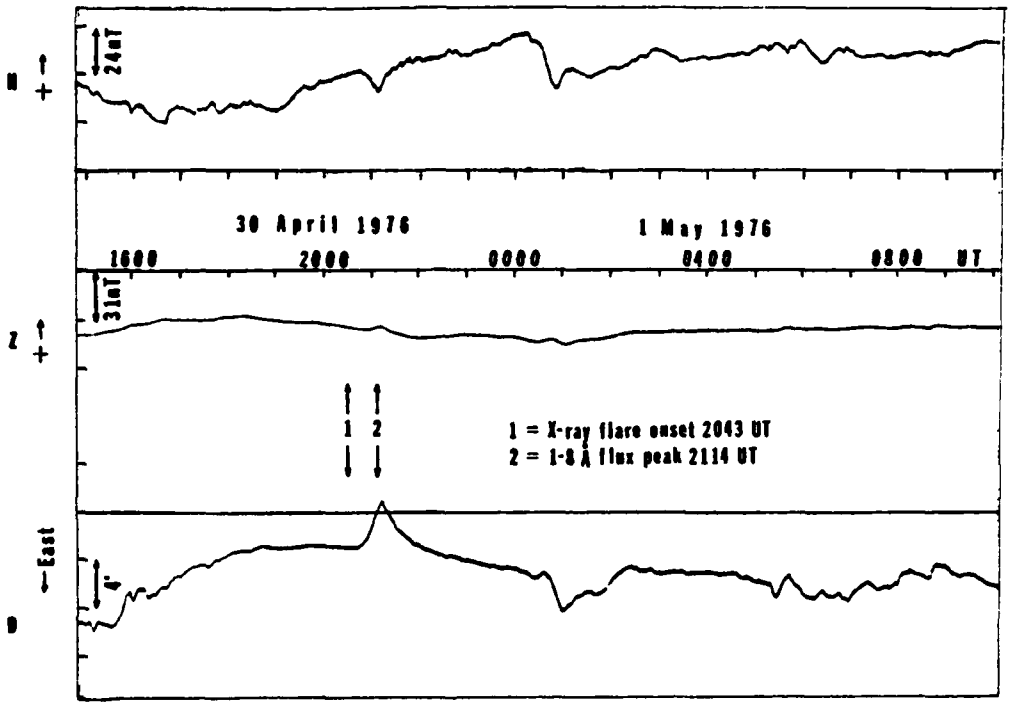

FIGURE 13 Boulder magnetogram showing the solar flare effect at about 2100 UT 30 April 1976.

The location of the flare at longitude W45, or about 3 days past central meridian, placed the Earth at a point connecting it to the sun along the garden-hose shaped interplanetary magnetic field lines. The onset of a ground-level event was in fact detected between 2120 and 2125 UT by the Inuvik, Canada, neutron monitor (Shea, 1977). A polar cap absorption (PCA) beginning between 2125 and 2130 UT was observed at Thule, Greenland (Turtle et al., 1977), and at several high latitude soviet stations (Driatsky et al., 1977). The latter group found that the PCA onset in the southern polar regions was delayed by about 6½ hours after the PCA onset in the northern hemisphere. The onset of 6-10 MeV protons were observed on SMS/GOES at 2130 UT, and maximum polar cap absorption at Thule reached 2.7 dB at 0120 UT on 1 May (Shea, 1977). The interplanetary magnetic field direction (as measured by IMP-8) was generally toward the sun at flare time and until after 0600 UT 1 May 1976. Thus, these Soviet results appear to contradict a simple interconnection magnetosphere model, where energetic protons would have direct (indirect) access to the southern (northern) polar cap.

A decrease of 20 km in the VLF reflection height coincident with the increased riometer absorption at Thule was reported by Turtle et al. (1977). An SPA is also evident in this data at about 2100 UT. Thus, it

is not obvious whether the sudden reflection height drop was primarily caused by photon or particle ionization.

In Chapter 2 it was shown that travelling interplanetary shock waves are associated with high energy proton producing flares and Types II and IV radio bursts. The Helios-2 spacecraft at 0.43 AU and Helios-1 at 0.67 AU did observe solar wind velocity, temperature, and density discontinuities following the 30 April solar flare (Figures 14 and 15; Schwenn et al., 1977). The observed density decrease and velocity increase with time are consistent with the MHD jump conditions for an oblique shock. However, from the time of arrival of the discontinuities at Helios-1 and Helios-2, Schwenn et al. (1977) concluded that a tangential distontinuity, corotating with the sun, was observed. In any case, these two spacecraft were almost on the opposite side of the sun from the Earth, showing the widespread extent of the shock front.

4.4 The Ionospheric Storm

The major variations in the ionosphere during geomagnetic storms take place mainly in the F region and above (Matuura, 1972). Ionospheric storm-time disturbances are operationally significant if they have an effect on the systems which rely on the transit of radio waves through the ionosphere, such as over-the-horizon

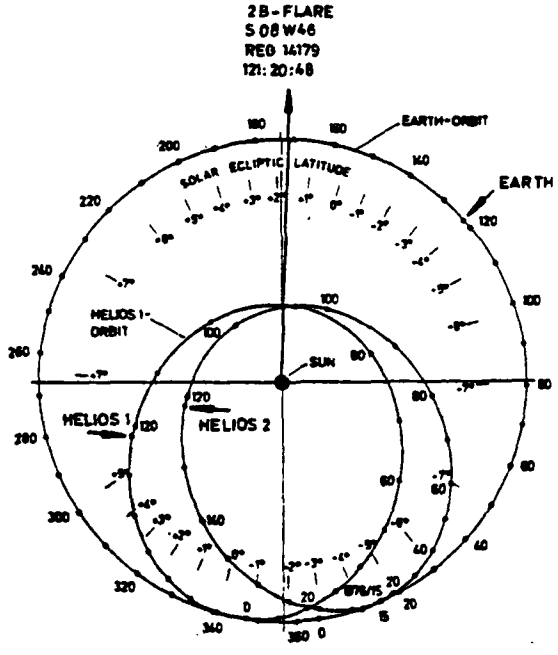

FIGURE 14 The positions of the Earth, Helios-1, and Helios-2, and the longitudinal location of the major flare on day 121 (30 April 1976) (Schwenn et al., 1977).

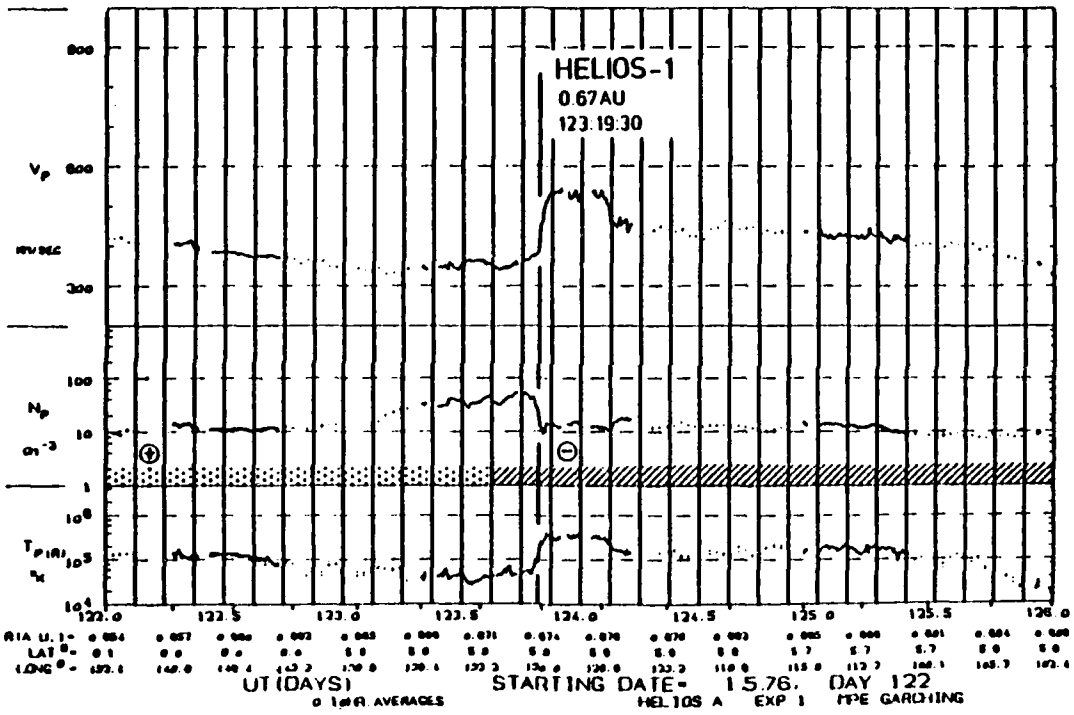

FIGURE 15 Solar wind proton velocity, V_p, density, N_p, and temperature, T_p, measured by Helios-1 for days 122 to 126 (1-5 May 1976, UT). The discontinuities on day 123 (2 May 1976) at about 1930 UT are indicated (Schwenn et al., 1977).

radar and communication systems and satellite communication links. The primary objective of this section is to investigate the behavior of F-region electron concentration during a period of intense study of solar-terrestrial interactions by the international scientific community. The available data were analyzed and presented to give some insight into the relationship of ionospheric variations to geomagnetic storms. In this way a better understanding of magnetospheric-ionospheric interactions might be obtained. One ultimate goal of such studies is to increase the reliability of forecasting disturbances and their impact on systems operating in the ionospheric environment.

In order to discuss the storm behavior of F-region peak electron density (NmF2), the critical frequency of the F2 region (foF2) was analyzed (where foF2 is proportional to the square root of NmF2). The first requirement in analyzing the ionospheric storm behavior is to determine the general background variations, or "non-storm" behavior. The variations due to the storm can then be identified. The method used here is now described.

Median foF2 for 72 ionospheric stations (Figure 16, Table I) distributed around the world was obtained, or calculated using foF2 data, from WDC-A for the period 30 April to 5 May 1976. The median foF2 was plotted

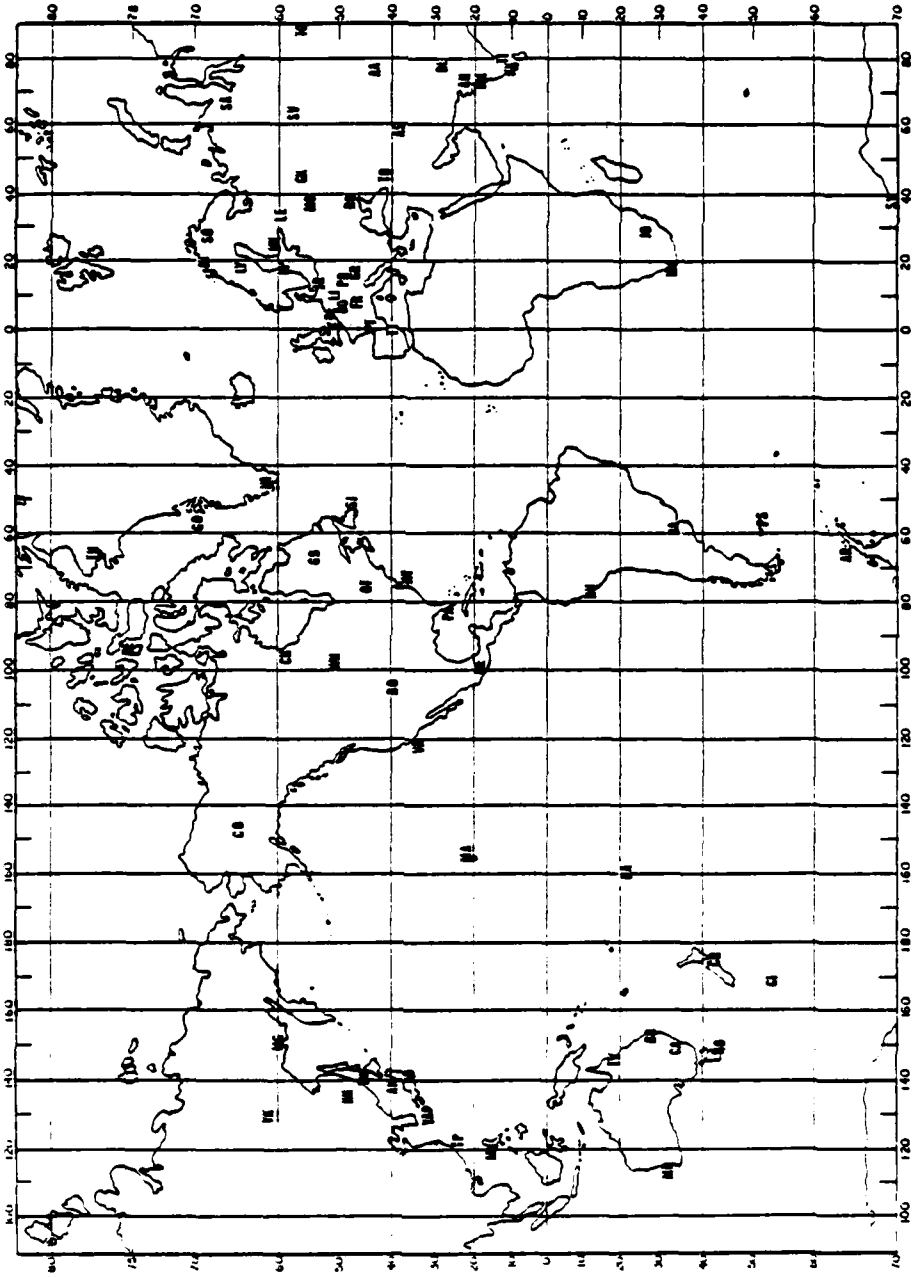

FIGURE 16 Mercator projection of a map of the 72 ionospheric stations used in this study in geographic coordinates.

according to local time for each station and reviewed for consistency with previous studies. Sample median foF2 plots are displayed in Figure 17 for College, Alaska (+64.7° lat., 256.5° long., geomagnetic), and Mexico City, Mexico (+29.1° lat., 326.8° long., geomagnetic). Both stations were in northern hemisphere summer, but the diurnal curves for these stations were quite different. The F region above College was sunlit 24 hours a day and the hourly values were fairly constant at about 4 MHz. The enhancement seen at 0300 LT may have been due to the small data set at College from which to select a median (due to frequent blackouts of the ionosonde signal) rather than due to any actual physical mechanism. The effect of the solar zenith angle was much more apparent at Mexico City, where the afternoon enhancement reached over 9 MHz before rapidly dropping around sunset. In general, the variations at these stations were consistent with the discussion by Rishbeth and Garriott (1969, p. 175-186).

The worldwide, or global, behavior of the F region is more symmetric about the geomagnetic rather than geographic equator (UAG-10 Report). This is an indication of the strong dependence of ionospheric dynamics upon the Earth's magnetic field. Martyn (1959) obtained the average local time behavior of NmF2 for sunspot minimum, 1943-44, and sunspot maximum, 1947, for both

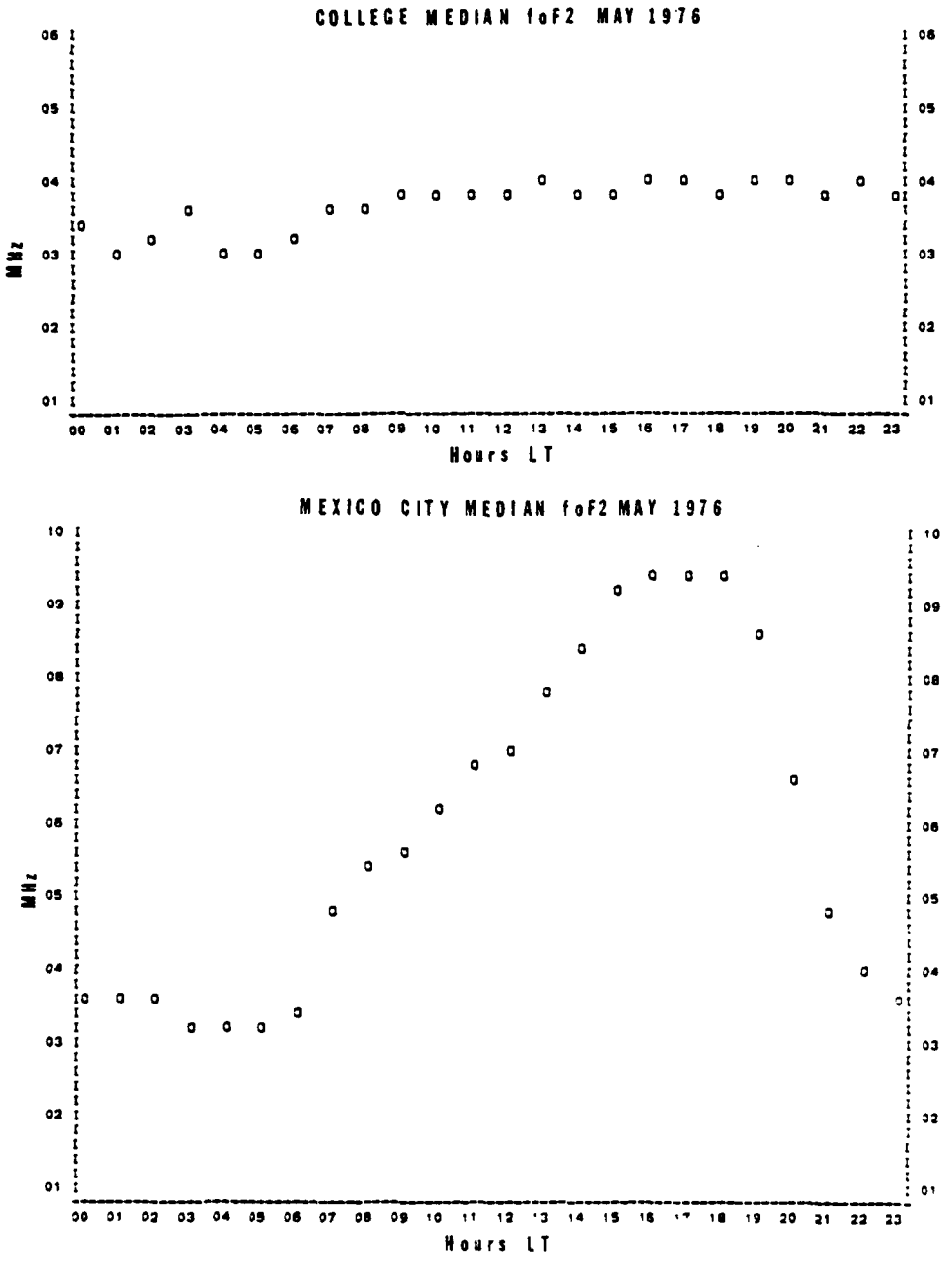

FIGURE 17 Median foF2 for May 1976 versus local time for College, Alaska (+64.7° lat., 256.5° long., geomagnetic) and Mexico City, Mexico (+29.1° lat., 326.8° long., geomagnetic).

equinox and summer solstice. Contours of equal electron density at the F2 peak were plotted in geomagnetic coordinates versus local time to show the diurnal variation at a given geographic longitude (Figures 18 and 19). Alternately, these figures may be taken to represent a snapshot of the global NmF2 median values with the subsolar meridian at 1200 LT. The F-region ionization was found to be generally more enhanced during solar maximum as would be expected. It was also more enhanced during equinox than summer solsice, during both solar maximum and minimum.

For this study similar contours were drawn for median foF2, again, proportional to $(NmF2)^{\frac{1}{2}}$, for May 1976. First, the median values were arranged according to local time at each station, and stations were arranged in 10^{o} geomagnetic latitude bands. Then, the values at each local hour for each latitude band were averaged and 16 values were obtained (no stations were in the -10^{o} to -20^{o}, or -80^{o} to -90^{o} latitude bands). Contours were drawn at 1 MHz intervals and displayed for 0000 to 2300 local time (Figure 20). It is suspected that missing data in the -10^{o} to -20^{o} geomagnetic band more seriously affected the median foF2 field than the absence of data in the -80^{o} to -90^{o} band. This is evident from the steeper gradients in foF2 found at the lower latitude bands in the northern hemisphere, and

1943-44
SUNSPOT MINIMUM

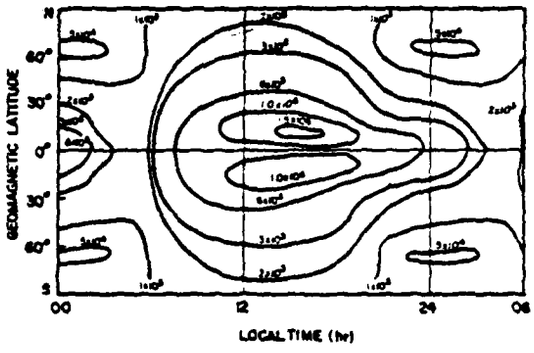

Equinox

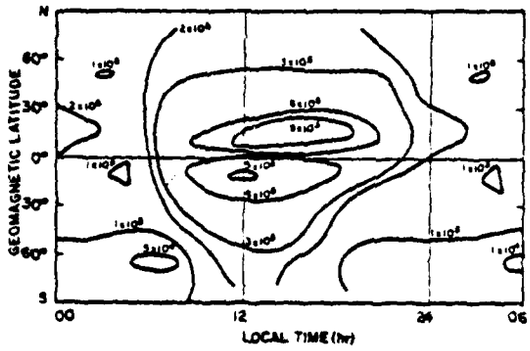

Summer Solstice

FIGURE 18 Contours of average NmF2 in electrons cm^{-3} [proportional to $(foF2)^2$] at equinox and summer solstice during sunspot minimum, 1943-1944 (Martyn, 1959).

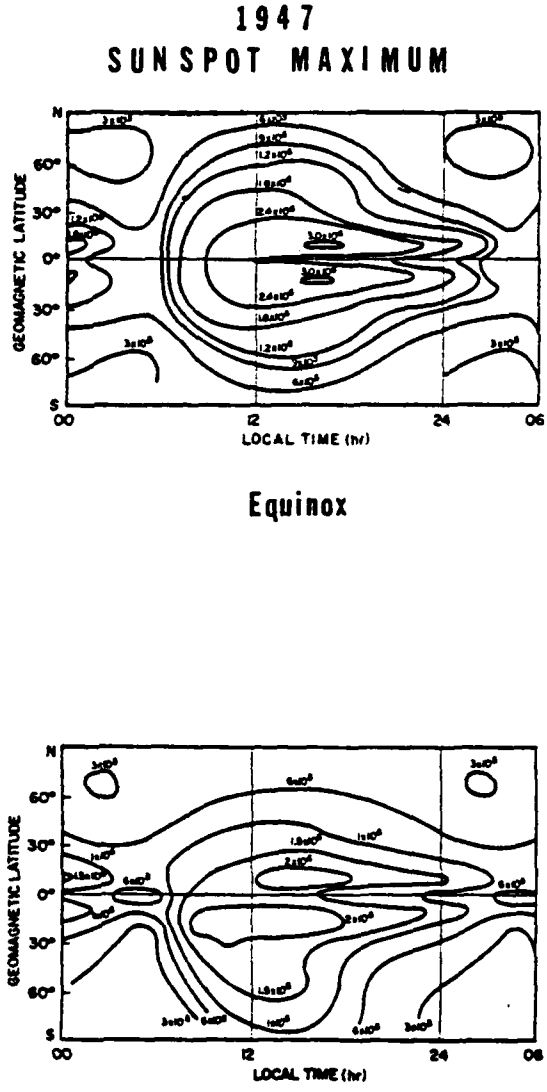

FIGURE 19 Contours of average NmF2 in electrons cm^{-1} [proportional to $(foF2)^2$] at equinox and summer solstice during sunspot maximum, 1947 (Martyn, 1959).

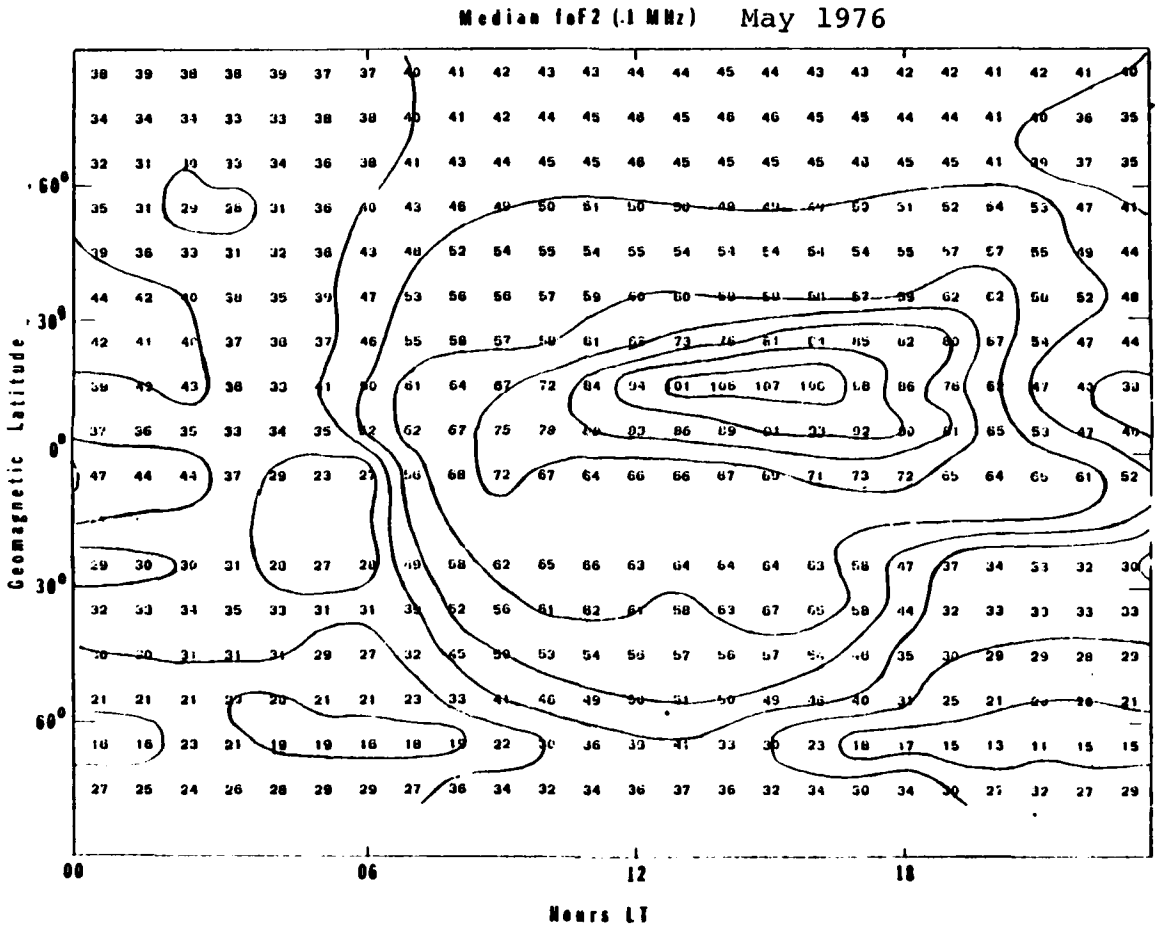

FIGURE 20 Contours of median foF2 for May 1976 versus local time. Values are averaged around 10^{o} geomagnetic latitude bands for each local hour. Contours of equal foF2 [proportional to $(NmF2)^{\frac{1}{2}}$] are at 1 MHz intervals.

expected in the low latitude southern hemisphere, from a comparison with Martyn's (1959) results.

Comparisons of Figure 20 with Figures 18 and 19 shows that median foF2 (and thus NmF2) for May 1976, at sunspot minimum, shows a better agreement with Martyn's (1959) NmF2 pattern during sunspot maximum, 1947. The increase in solar activity during March to May 1976 may be responsible for this. The double peaks in Figure 19 at the low latitude afternoon are replaced by a peak at $+10^{\circ}$ to $+20^{\circ}$ geomagnetic latitude in Figure 20. Again, missing data in the -10° to -20° band may account for the absence of a southern peak. The limited data set for May 1976, and differing solar conditions, may be responsible for other differences in the figures. However, the general features shown in Figure 20 agree with what one would expect for the actual ionosphere, i.e., peak ionization at low latitudes in the afternoon, with rather small high latitude diurnal variations.

The hourly values of ΔfoF2 (defined in section 3.2) were averaged at each hour universal time during the study period using the data from all 72 ionospheric stations. The absolute values of averaged ΔfoF2 were generally .1 MHz from the beginning of the storm period (1800 UT 30 April) to 1800 UT 2 May. The average of all values was near zero. This exercise provided some confidence in the view that median foF2 for May 1976

might approximate the non-storm behavior of foF2 in the early part of May 1976.

The geomagnetic field throughout 30 April to 5 May 1976 was under the influence of a 27-day recurring enhancement as shown by the Ap index graph in Figure 5. Common-scale magnetograms for 11 stations listed in Table II during the period 1200 UT 1 May to 1200 UT 3 May are displayed in Figure 21 (from SGD, 1976). The diurnal variation has been subtracted out, leaving the disturbance variations in the horizontal components of the geomagnetic field. Also shown in Figure 21 are the high latitude disturbance indices AU and AL. AU and AL are the upper and lower envelopes of superimposed high latitude H-component magnetograms, using the stations Leirvogur, Fort Churchill, College, Tixie Bay, and Dixon Island. AE is the difference between the two envelopes and gives quantitative values for the intensity of the auroral electrojet current, in units of gammas (Davis and Sugiura, 1966).

Disturbances in nearly all the magnetograms at about 0300 UT and 1200 UT on 2 May, preceded the SSC at 1829 UT on the same date. This SSC was not associated with typical initial, main, and recovery geomagnetic storm phases. Badillo (1977) compared the 2 May 1976 SSC with two previous cases on 26 March and 1 April 1976 (Figure 22) at the geomagnetic equatorial station in

TABLE II

LIST OF GEOMAGNETIC STATIONS BY GEOMAGNETIC LATITUDE

Station	Geographic		Geomagnetic	
	Latitude	Longitude	Latitude	Longitude
Thule	77.48	290.83	86.78	36.26
Resolute Bay	74.70	265.10	84.14	304.32
Fort Churchill	58.80	265.90	70.27	316.01
Dixon Island	73.55	80.57	68.31	154.69
Leirvogur	64.18	338.30	66.82	69.54
Tixie Bay	71.58	129.00	65.82	195.48
College	64.87	212.17	64.83	259.65
Boulder	40.13	254.77	49.49	315.70
San Juan	18.12	293.85	31.46	5.54
Kakioka	36.23	140.18	29.92	209.88
Davao	7.08	125.58	-4.00	194.97
Hermanus	-34.42	19.23	-41.46	79.72

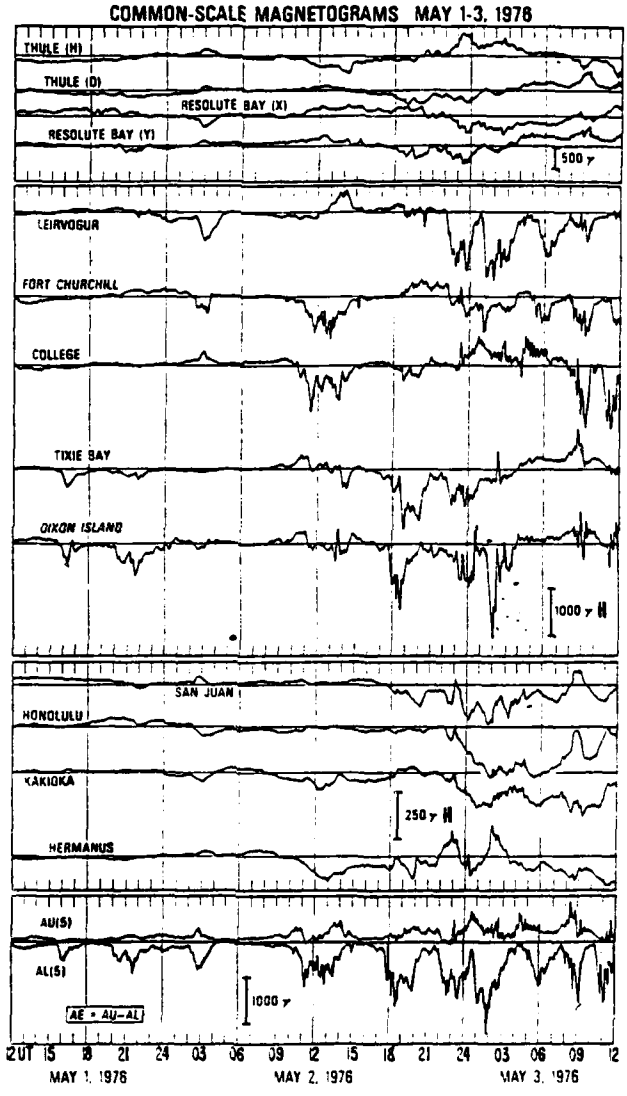

FIGURE 21 Common-scale magnetograms for 1-3 May 1976 (SGD, 1976).

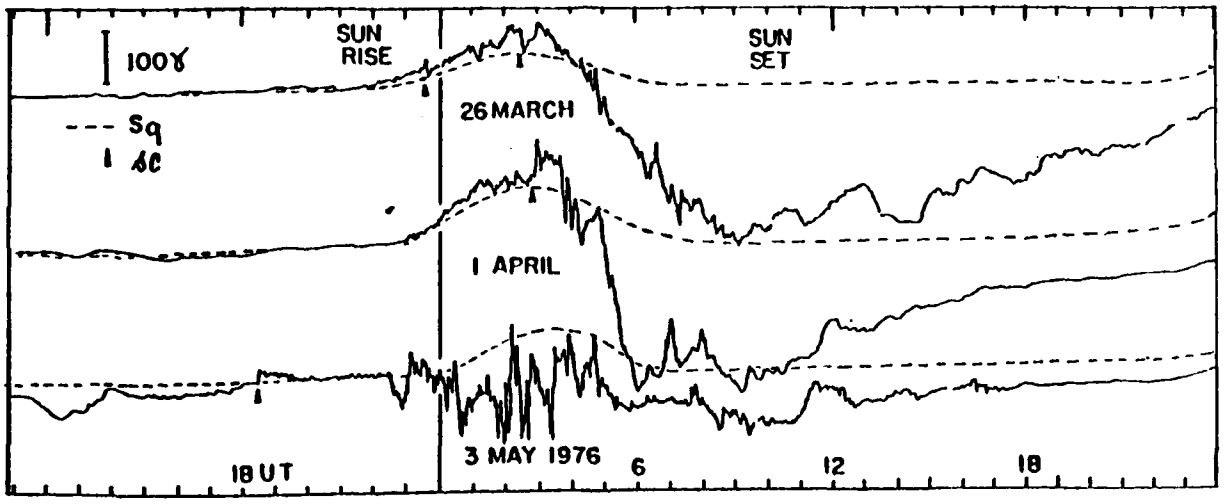

FIGURE 22 H-component magnetograms at Davao (04°S latitude, 195° longitude, geomagnetic) during 20 March to 3 May 1976. Storm sudden commencements are indicated by arrows and average diurnal behavior (Sq) by dashed lines (from Badillo, 1977).

Davao, Philippines. The earlier two SSCs were followed by initial increases over the diurnal curve in the H-component magnetograms, followed several hours later by a large decrease, and then a slow recovery over the next day or so to pre-SSC values. The 2 May SSC initial phase increase was considerably smaller at Davao, and the main phase decrease was not clearly defined for another 6 hours or so. Also, the maximum decrease in the H-component was much less than during the other two storms.

Deviations of hourly foF2 from monthly medians for each of the 72 ionospheric stations were plotted according to universal time to aid in determining the global behavior of the ionosphere during the study period. Graphs of ΔfoF2 were ordered by longitudinal region (i.e., Austro-Asian, North-South American, Eurasian, and Pacific) and then stacked by geomagnetic latitude. The same frequency scale was used on all graphs. Sample stacked ΔfoF2 plots are shown in Figures 23 to 29. High, middle, and low geomagnetic latitudes are represented, with the exception mentioned before, that no data was available in the -10° to -20°, and -80° to -90° latitude bands. For the purpose of the discussion here, the study period has been divided into the part before the geomagnetic SSC, the pre-storm period (30 April, 1800 UT to 1830 UT, 2 May 1976), and the part following the SSC, the storm period (1830 UT, 2 May to 2300 UT, 5 May 1976).

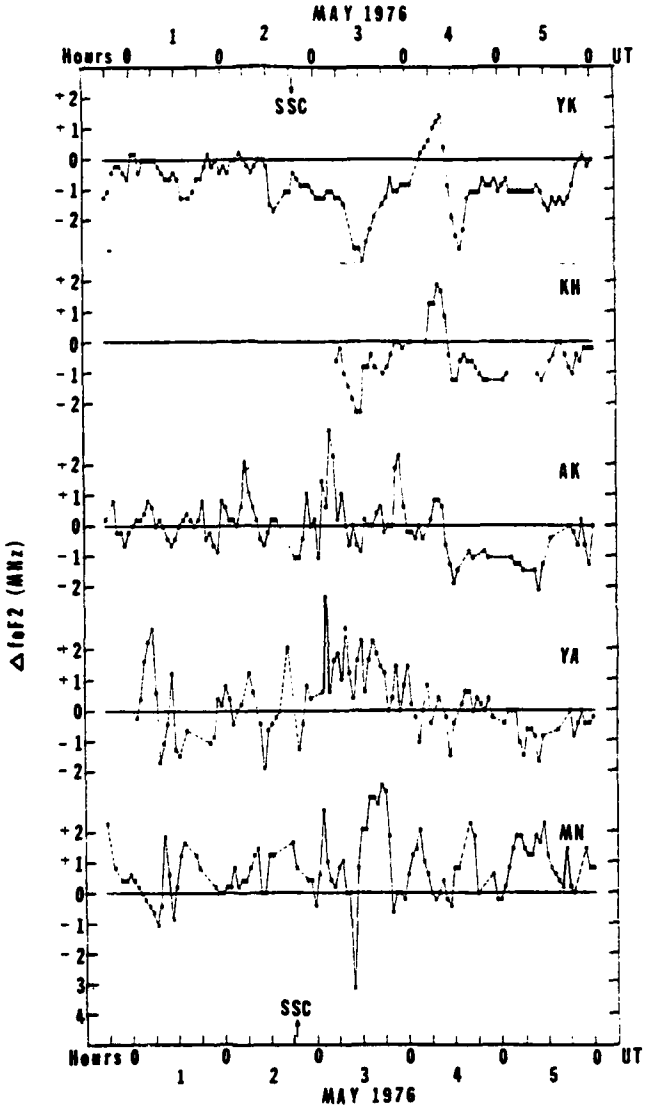

FIGURE 23 Deviations of hourly foF2 from monthly median values during the period 1800 UT on 30 April to 2300 UT on 5 May 1976 for the stations Yakutsk, Khaborovsk, Akita, Yamagawa, and Manila (Austro-Asian sector).

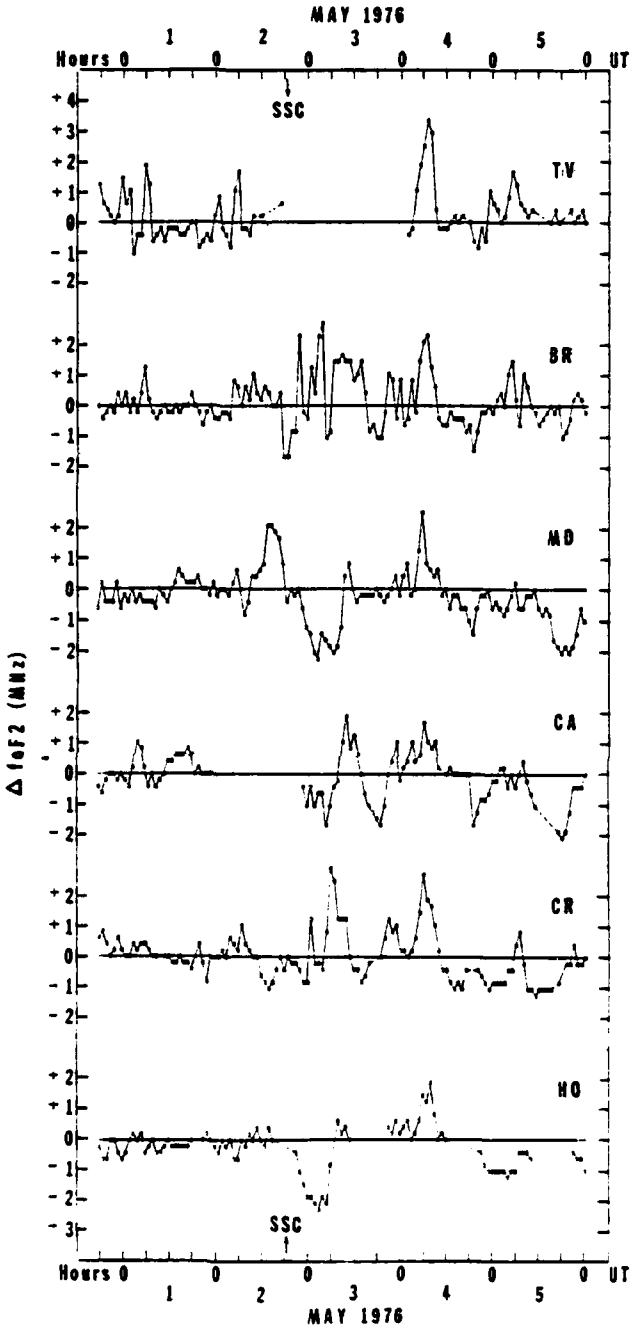

FIGURE 24 Deviations of hourly foF2 from monthly median values during the period 1800 UT on 30 April to 2300 UT on 5 May 1976 for the stations Townsville, Brisbane, Mundaring, Canberra, Christchurch, and Hobart (Austro-Asian sector).

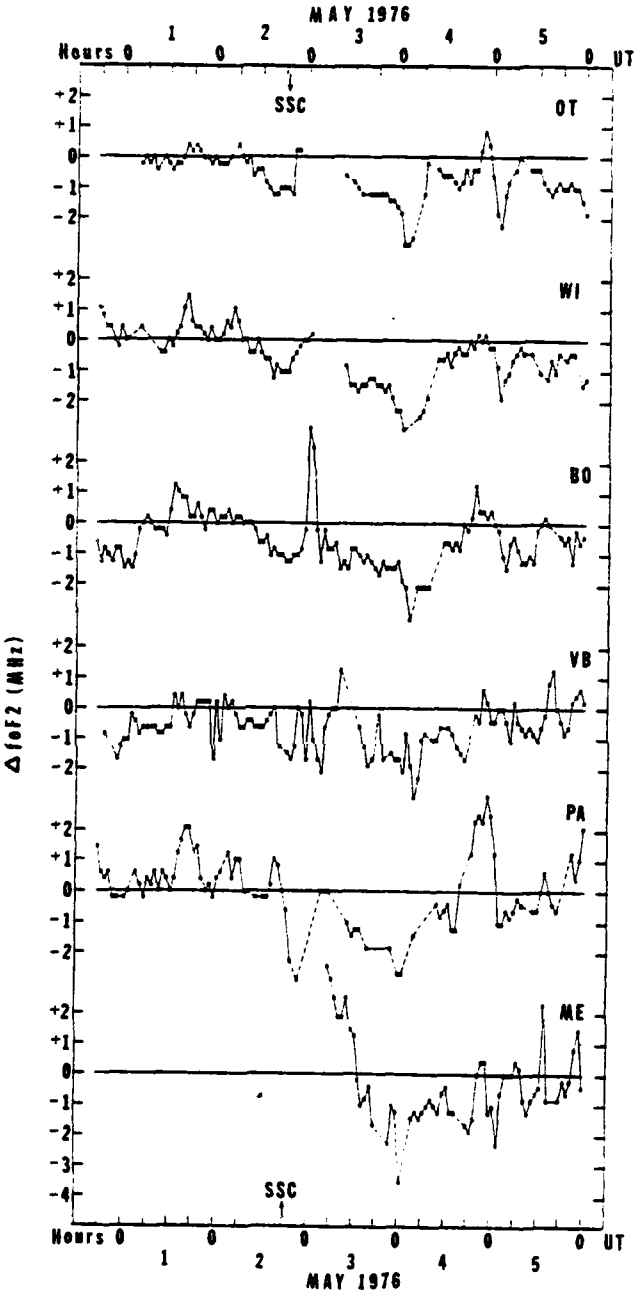

FIGURE 25 Deviations of hourly foF2 from monthly median values during the period 1800 UT on 30 April to 2300 UT on 5 May 1976 for the stations Ottawa, Wallops Island, Boulder, Vandenberg AFB, Patrick AFB, and Mexico City (N-S American sector).

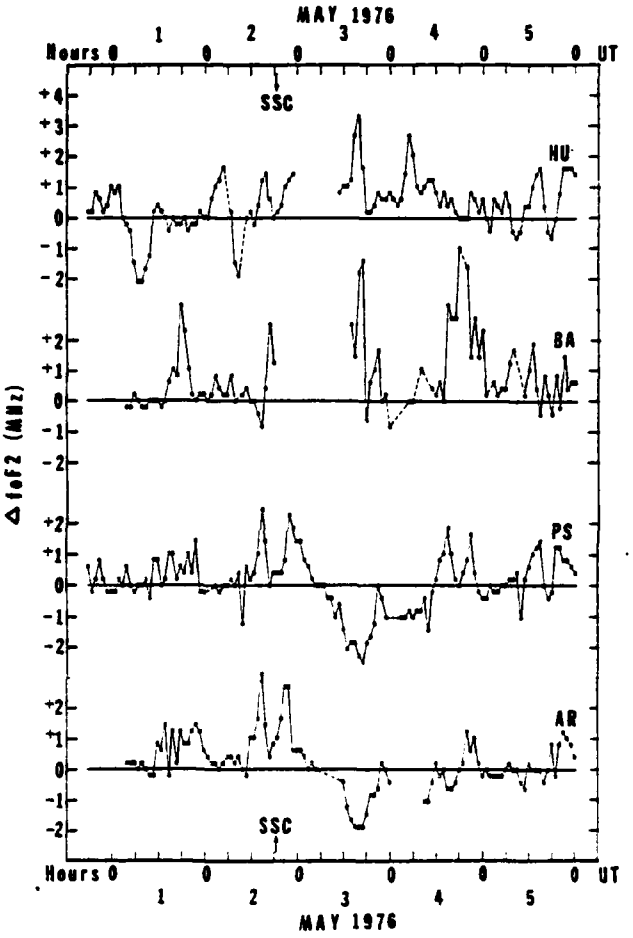

FIGURE 26 Deviations of hourly foF2 from monthly median values during the period 1800 UT on 30 April to 2300 UT on 5 May 1976 for the stations Huancayo, Buenos Aires, Port Stanley, and Argentine Island (N-S American sector).

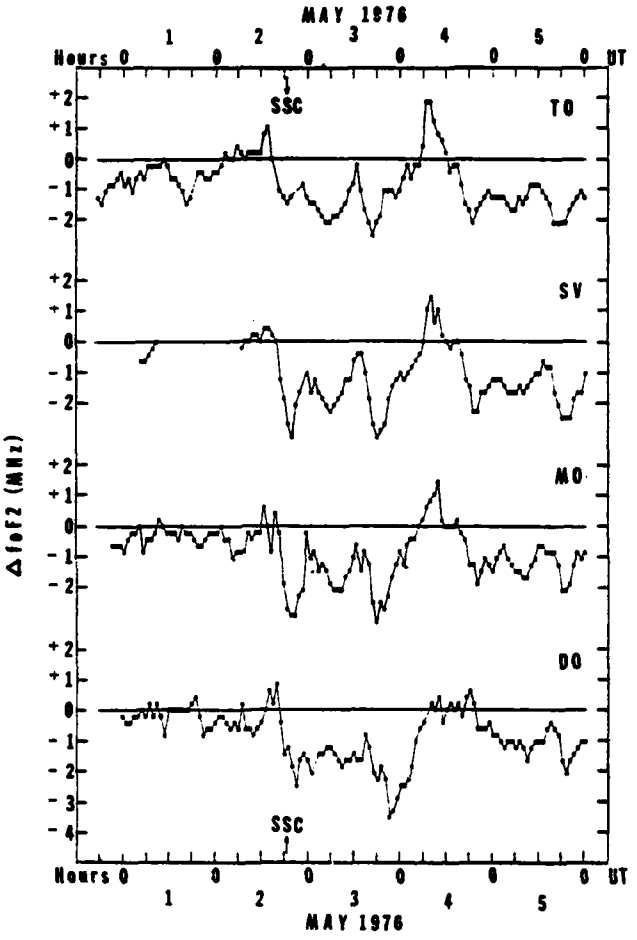

FIGURE 27 Deviations of hourly foF2 from monthly median values during the period 1800 UT on 30 April to 2300 UT on 5 May 1976 for the stations Tomsk, Sverdlovsk, Moscow, and Dourbes (Eurasian sector).

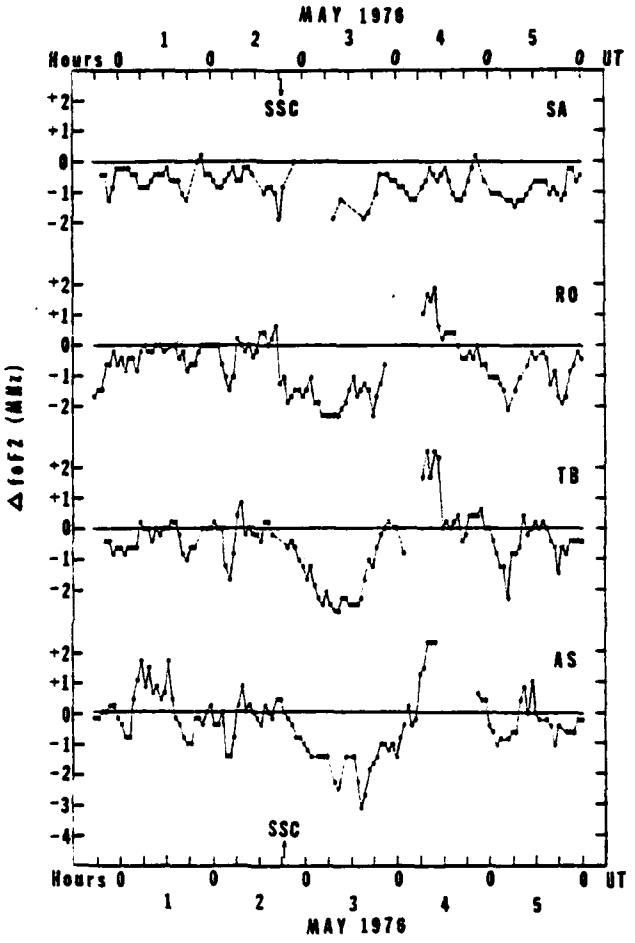

FIGURE 28 Deviations of hourly foF2 from monthly median values during the period 1800 UT on 30 April to 2300 UT on 5 May 1976 for the stations Salekhard, Rostov, Tblisi, and Ashkhabad (Eurasian sector).

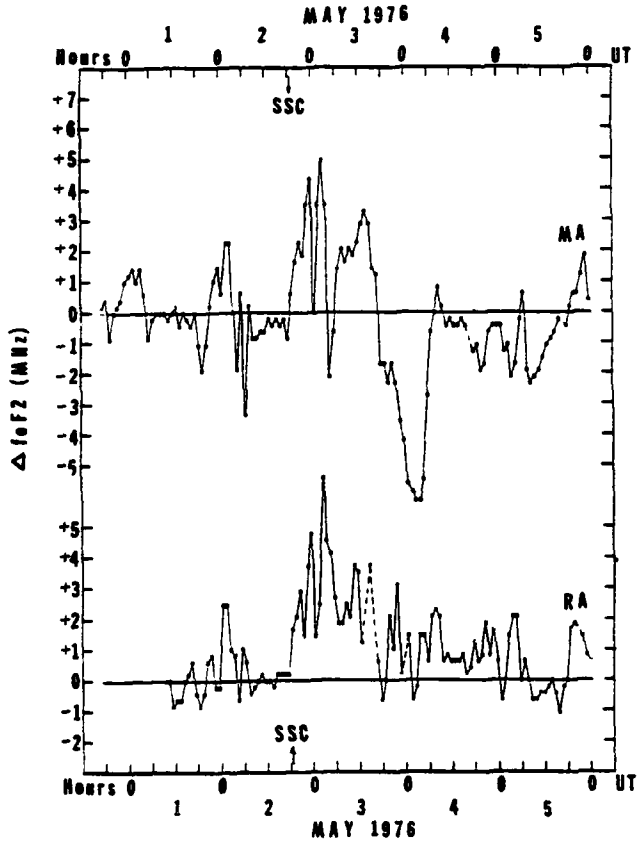

FIGURE 29 Deviations of hourly foF2 from monthly median values during the period 1800 UT on 30 April to 2300 UT on 5 May 1976 for the stations Maui, and Raratonga (Pacific sector).

The general behavior of the pre-storm ionization in the F region was fairly close to the median for May. This is shown by the relatively small ΔfoF2 values for most stations. Exceptions existed at low geomagnetic latitude stations, examples being Manila (5.1°N) and Yamagawa (20.3°N) in Figure 23, Townsville (28.5°S) in Figure 24, and Huancayo (0.6°S) and Buenos Aires (23.2°S) in Figure 26. In these cases it appears that the pre-storm ionization in local afternoon was enhanced above normal, while depressed below normal during local night-time. This corresponds in time with the slightly unsettled geomagnetic field. (The daily averaged Ap value was 10 on 30 April and 1 May, and daily averaged Dst fell to -22 and -10 gammas.) It may also be the case that subtracting the May median foF2 was not entirely successful in removing the diurnal variations at the low latitude stations on the pre-storm days.

An interesting feature of the pre-storm foF2 in the Eurasian sector (Figure 27) is the small (∿1 MHz) enhancement around 1600 UT on 2 May 1976, shortly after the geomagnetic substorm disturbance at about 1100 to 1400 UT. The Leirvogur (Eurasian sector) magnetogram in Figure 21 (SGD, 1976) and the 15-minute interval AE index in Figure 30 (IAGA Bulletin No. 32g) show the substorm occurrence. The ΔfoF2 behavior in the Eurasian sector can be seen in Figure 27. The initial enhancement

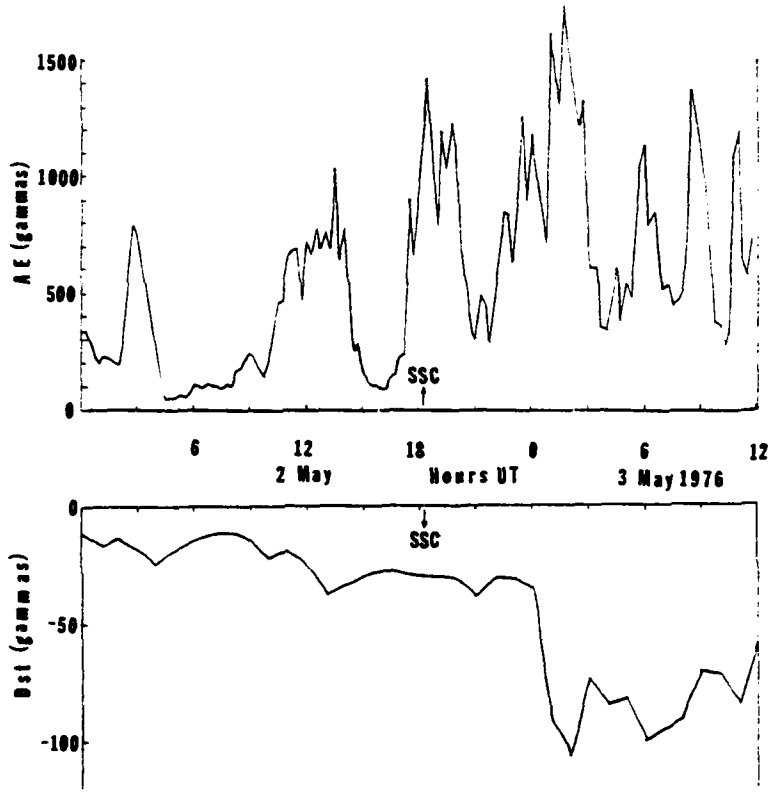

FIGURE 30 Preliminary AE(5) index at 15-minute intervals (data from IAGA Bulletin no. 32g) and hourly averaged Dst (SGD, 1976) for 0000 UT 2 May to 1200 UT 3 May 1976.

was rapidly followed at about 1700 UT by larger negative values of ΔfoF2, reaching -2 to -3 MHz at about 2000 to 2100 UT, on 2 May. This feature can perhaps be explained in terms of the storm-time equatorward neutral winds mentioned in Chapter 2. However, in this case, the ΔfoF2 changes appear to be associated with a specific substorm before the SSC. More will be said about this in the storm mechanism discussion in the following chapter.

The N-S American sector (Figures 25 and 26) showed a generally negative trend in ΔfoF2 beginning at about 1200 UT on 2 May 1976. The initially positive phase seen in the Eurasian sector was not obvious in the other sectors.

A roughly 12-hour ΔfoF2 oscillation was observed during the pre-storm period at Akita on 30 April and 1 May with peaks in ΔfoF2 at about 1 MHz (Figure 23). This oscillation was also seen on 1 May at Canberra (Figure 24) and at Wallops Island (Figure 25) in the N-S American sector on 1 and 2 May. The 15-minute ΔfoF2 data at Moscow and Rostov experienced oscillations during local daytime on 2 May with the best defined peaks and troughs with periods of 2-1/4 to 3-3/4 hours. Similar oscillations were observed in Maui's 15-minute ΔfoF2 during the the pre-storm period. Between 0300 and 0500 UT (1700 and 1900 LT) on 2 May, ΔfoF2 dropped by

4 MHz. A period of about 3-3/4 hours was determined associated with these variations. Noting that geomagnetic substorm activity occurred at about 0300 UT on 2 May (Figure 29), it may be assumed that these oscillations are evidence of TID passage at these stations. It should be pointed out that the shortest oscillation periods which can be resolved from a sampling rate at interval T, is 2T. Thus, the 15-minute data cannot reliably resolve period shorter than one-half hour, while the resolvable period increases to 2 hours when using hourly ΔfoF2. Discussion of other oscillatory features will be continued in Section 3.5.

The most clearly defined positive ionospheric storm phase following the geomagnetic SSC at 1830 UT on 2 May 1976 was in the Pacific sector (Figure 29). The oscillatory ΔfoF2 was enhanced at about 0300 UT (1700 LT) at Maui and Raratonga by 5 and 6 MHz, respectively. The onset of the geomagnetic storm initial phase was not very spectacular, as can be seen from the hourly Dst for 0000 UT on 2 May to 1200 UT on 3 May 1976 in Figure 30 (SDG, 1976). However, the SSC was followed 6 hours later by an extremely abrupt decrease in Dst of 80 gammas. Shortly afterward, a major disturbance in F-region ionization took place on the day-side hemisphere. The Boulder ΔfoF2 increased by over 4 MHz between 0000 and 0100 UT on 3 May (Figure 25). Many stations were

unable to scale F-region parameters for several hours around 0000 UT on 3 May due to range or frequency spreading of the ionosonde trace (caused by electron density anisotropies, or gradients) or due to blackout. Notice the lack of ΔfoF2 data during this period at Ottawa, Patrick AFB (Figure 26), Huancayo, and Buenos Aires (Figure 27). A sharp peak in 15-minute foF2 and ΔfoF2 an Manila around 0145 UT was followed by peaks at Taipei and Yamagawa at 0245 UT (Figures 31 and 32). This peak may have been due to a poleward propagating gravity wave, as will be discussed in Section 3.5.

Jackowski and Lazo (1977) reported that between 0000 and 0900 UT on 3 May 1976, the SMS-1 Faraday electron content measurements at Havana were "heavily disturbed by an unknown origin." Unusually high scintillations at Chung-Li, Taiwan, during this period can be seen in the data presented by Huang (1977). This disturbance was followed at Havana by a large reduction in Faraday electron content in the local afternoon on the same day (50% reduction at 1900 UT on 3 May 1976). Enhancements of Faraday electron content were measured between 0200 and 0500 UT on 3 May at Goose Bay, Labrador (+64.6 lat., 12.1 long., geomagnetic) and Patrick AFB, Florida (+39.4 lat., 347.3 long., geomagnetic) reaching several-hundred percent above pre-SSC values. An increase of 100% at Osan, Korea (+32.3 lat., 197.4 long.,

geomagnetic) was observed at 0400 UT while Athens, Greece (+36.5 lat., 101.9 long., geomagnetic), in the Eurasian sector showed no enhancements in Faraday electron content.

Although a positive phase to the ionospheric storm was not obvious, a clearly defined negative phase could be seen in the higher latitude station graphs (Figures 25, 26, and 27). The greatest negative values in ΔfoF2 in this study occurred during local evening on the first or second storm day. See, for example, the ΔfoF2 graphs for Maui at 0300 UT on 4 May, or 1700 LT (Figure 29), Boulder at 0200 UT on 4 May, or 1900 LT (Figure 25), and Moscow at 1800 UT on 3 May, or 2000 LT (Figure 27). There was a tendency for ΔfoF2 at mid-latitude stations to reach a daily maximum in the early afternoon and then to drop to the greatest negative values in about 3-4 hours. (See Figures 23 and 27.)

Close inspection of Figure 27 shows remarkable uniformity in the universal, or storm-time dependence of ΔfoF2 during the main phase at higher latitude stations, Tomsk, Sverdlovsk, Moscow, and Dourbes at geographic longitudes 84,9E, 61.1E, 37.3E, and 4.6E, respectively. Although the locations of these stations extend over a 80^{o} longitude range, the profiles of each graph are remarkably similar throughout 3 and 4 May. All stations are at roughly the same geomagnetic latitude.

The ΔfoF2 at lower latitude stations, such as Buenos Aires, Raratonga, and Yamagawa, was above zero on the average during the storm period (Figures 23, 26, and 29). This feature is more characteristic of winter storms than equinox or summer storms (Matsushita, 1959; Matuura, 1972). Also oscillatory variations in ΔfoF2 with periods of less than 2 to greater than 6 hours were seen at many stations. The most interesting of these oscillations appeared in the Austro-Asian sector. Fifteen-minute foF2 data for 1500 UT on 2 May to 1500 UT on 3 May in Figure 31 and ΔfoF2 data for 1500 UT on 2 May to 0800 UT on 5 May in Figure 32 are shown for the stations Wakkanai, Akita, Kokubunji, Yamagawa, Taipei, and Manila. Inspection of the figures shows a correspondence in the variations from station to station, although shifted in phase. The TID associated oscillations will be discussed in the next section. What appears to be a stationary wave in foF2 and ΔfoF2 can be seen shortly after F-region sunrise in Figures 31 and 32 for 3, 4, and 5 May at all 6 stations. Sunrise times are shown by the large dots in Figure 32. This morning peak appeared in the Faraday electron content measurements at Chung-Li on 3 May 1976, but was not pronounced on the following day (see Figure 3 from Huang, 1977). Although there is no obvious explanation of this peak, it may be due to a shock wave generated by the supersonic

AD-A106 427 AIR FORCE INST OF TECH WRIGHT-PATTERSON AFB OH F/G 4/1
IONOSPHERIC DISTURBANCES DURING THE PERIOD 30 APRIL TO 5 MAY 19--ETC(U)
MAY 79 C D FRY
UNCLASSIFIED AFIT-CI-79-284T-S NL

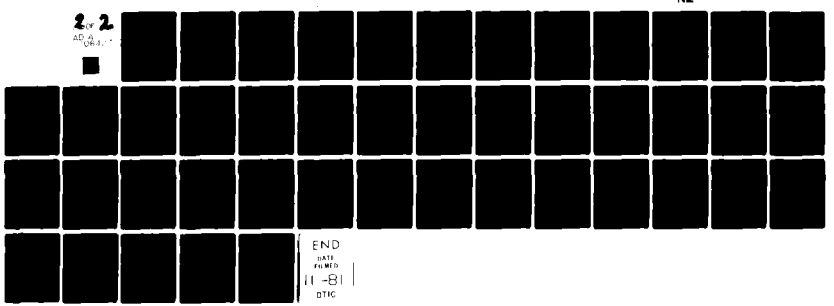

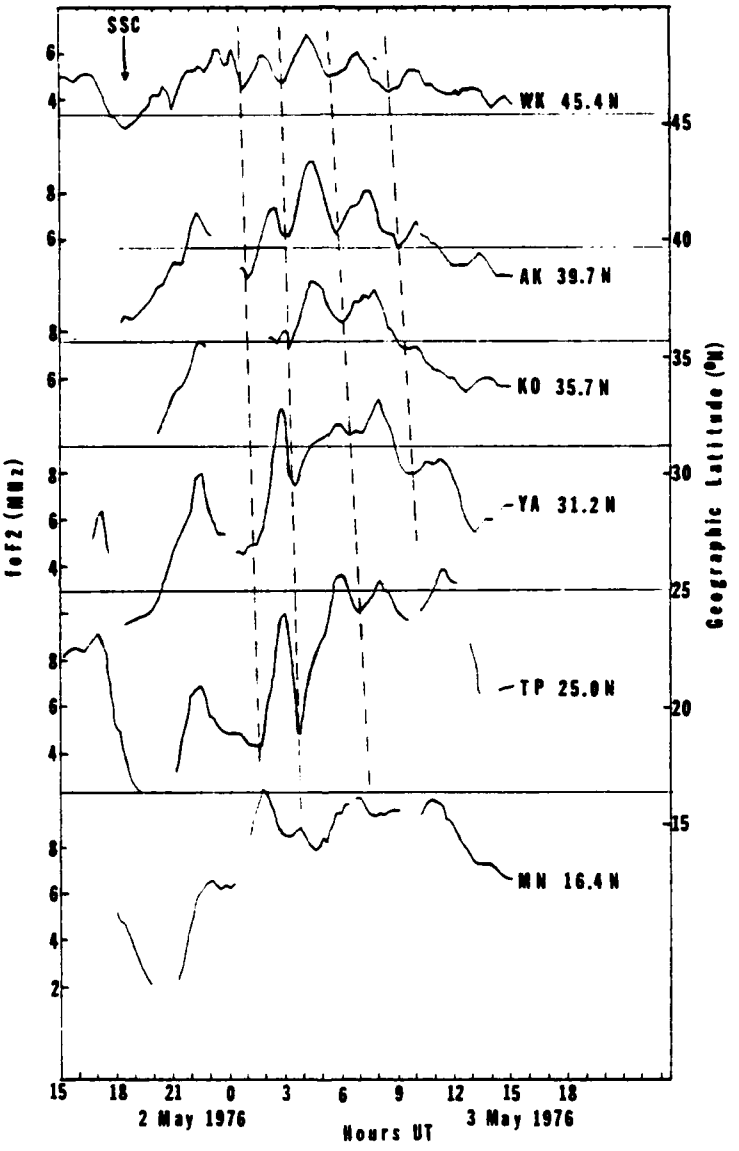

FIGURE 31 F2-layer critical frequency, foF2, for 1500 UT on 2 May to 1500 UT on 3 May 1976 for the station Wakkanai, Akita, Kokubunji, Yamagawa, Taipei, and Manila. Abscissas are spaced according to geographic latitude. Dashed lines indicate possible troughs of propagating ionospheric disturbances.

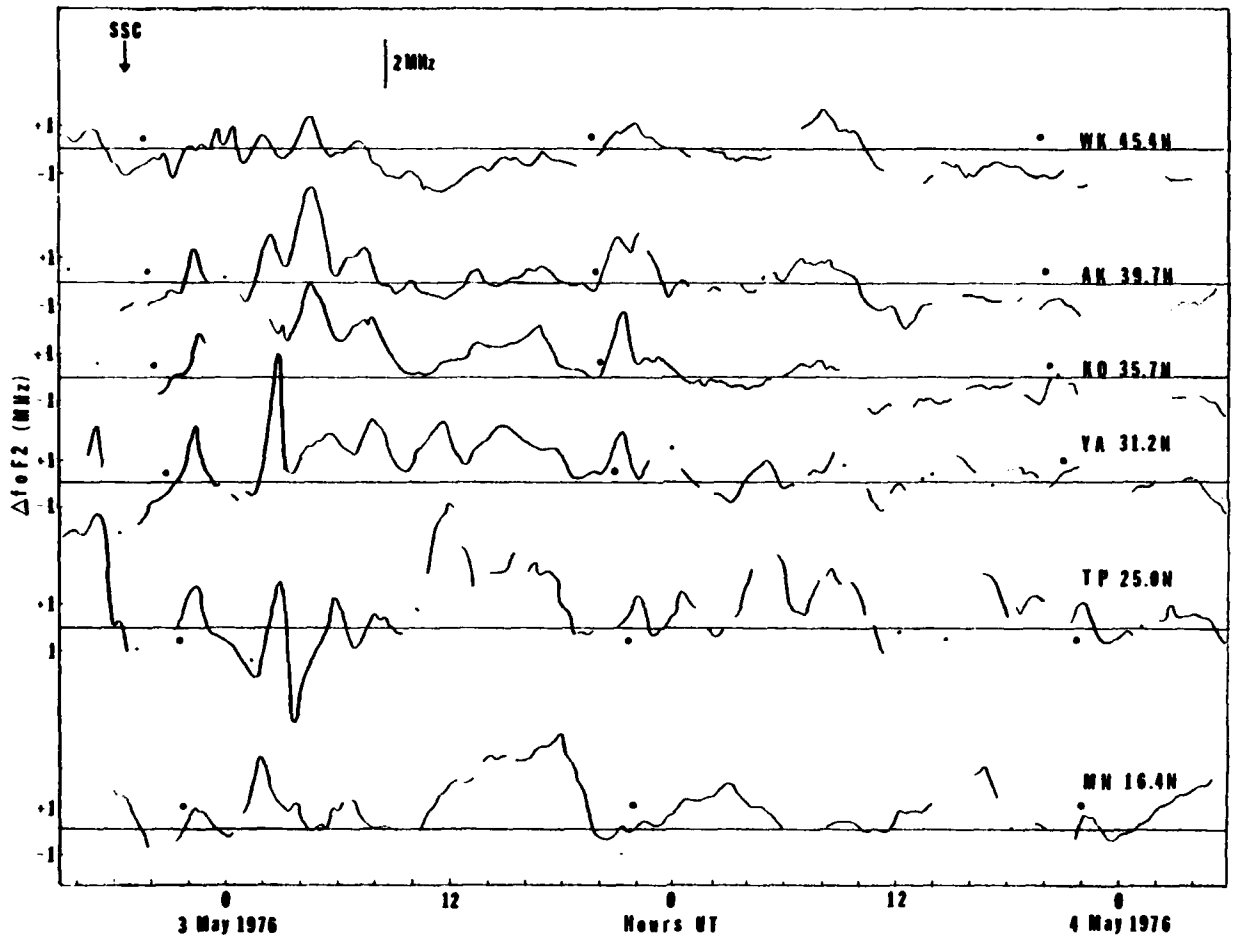

FIGURE 32 Deviations of foF2 from May monthly median for Wakkanai, Akita, Kokubunji, Yamagawa, Taipei, and Manila from 1500 UT on 2 May to 0800 UT on 5 May 1976. The SSC at 1829 UT on 2 May 1976 is indicated by the arrow, and local sunrise by solid dots. Abscissas are spaced according to geographic latitude.

velocity of the night-day terminator relative to the thermosphere (Francis, 1975). The post-sunrise peak has been observed in ATS-6 total electron content at Lindau and Graz on many days in 1975 and 1976 by Hartmann et al. (1976).

The largest variations in foF2 occurred in the Pacific sector during the main phase of the storm on 3 and 4 May 1976 (Figure 29) at Maui. This observation is interesting because this is precisely what Paul et al. (1977) found for the August 1972 storm events. The 4-5 August 1972 storm geomagnetic perturbations were largest in the Pacific sector. Comparison of the Honolulu magnetogram with those of other mid-latitude stations (Figure 21) indicates the same was true of the May 1976 storm geomagnetic variations. Maui and Raratonga, at geomagnetic conjugate points in Figure 29 show agreement in their ΔfoF2 behavior during the early storm period. (Note the peaks at 2100 UT on 2 May, 0000 UT and 0300 UT on 3 May.) However, by late 3 May, a -6 MHz ΔfoF2 had developed at Maui while the highly oscillatory ΔfoF2 at Raratonga averaged about +2 MHz. In other words, the local afternoon maximum foF2 was about 6 MHz at both stations. This indicates that during the main phase of the ionospheric storm, diffusion along conjugate geomagnetic field lines was from the summer to the winter hemispheres. Matsushita (1976) found this same result

for the August 1972 storm. Other stimilarities between that storm and the May 1976 storm will be discussed in Chapter 5.

Now that the major characteristics of the F-region peak ionization behavior have been discussed, it is worthwhile to list the most interesting features of the study period. They include:

1. Significant variations of ΔfoF2 ($\sim$2 MHz) occurred prior to SSC.

2. An "ionospheric substorm" occurred in the European sector following the 1200 UT 2 May geomagnetic substorm.

3. A clearly defined positive phase following the SSC was evident only in the Pacific sector. Also, the largest absolute values of ΔfoF2 occurred in the Pacific sector.

4. The clearly defined negative phase was most apparent in higher latitudes and in the local evening on the first storm day.

5. The lower latitude behavior was more characteristic of winter storms rather than summer storms.

6. A widespread F-region disturbance took place on the dayside hemisphere for at least the first 2 or 3 hours of 3 May 1976.

7. A post-sunrise foF2 peak appeared on the three storm days in the Austro-Asian sector.

8. A large number of travelling ionospheric disturbances moved through the mid-latitudes on the first storm day. The peaks and troughs in foF2 were greatest in the 20^{o} to 30^{o} geomagnetic latitude bands.

In summary, the general foF2 variations during the period of study were most characteristic of those associated with minor geomagnetic storms. This observation is consistent with the minor storm behavior of Dst. However, large geomagnetic substorm activity throughout 2 and 3 May 1976 appeared to be associated with abrupt changes in F-region ionization. In the next section some features of the travelling ionospheric disturbances are discussed and source regions are sought. The ionospheric storm features will be interpreted in terms of current theories in Chapter 5.

4.5 Travelling Ionospheric Disturbances

Francis (1975) summarized the characteristics of large scale travelling ionospheric disturbances as having horizontal speeds greater than the lower-atmospheric sound speed ($C \approx 300$ m sec^{-1}) and periods of 30 minutes to 3 hours and, generally, propagating from pole to equator. Conversely, medium scale TIDs travel at speeds less than the sound speed, have periods from 15 minutes to greater than an hour and, in general, the preferred direction is less distinct. Characteristics of long

period (2-3 hour) internal gravity waves are discussed in Appendix A.

Inspection of the 15-minute ΔfoF2 data available for the storm period shows several cases of periodic fluctuations which retained their structure at several stations along a meridian. Figures 31 and 32 show the series of oscillations in foF2 and ΔfoF2 in the Austro-Asian sector, particularly on 3 May. The spacing between abscissas of the graphs were drawn according to geographic latitudes. In this way meridional distances could be retained. Then, by simply drawing a line through a series of troughs or crests, the TID apparent horizontal velocity could be determined by dividing the meridional distance between abscissa intersects by the time difference between peaks or troughs. It is important to note that the apparent horizontal velocity is greater than the actual horizontal velocity (Davies and Jones, 1972). The assumption in this method is that the TID was propagating in the north-south direction. In other words,

$$V = \frac{\phi_2 - \phi_1}{T_2 - T_1} \quad , \quad \text{(degrees latitude/time)} \qquad (4.1)$$

where V is the TID horizontal velocity, $T_2(T_2)$ corresponds to trough or crest passage at the station with latitude $\phi_2(\phi_1)$. Possible TID passages are identified by the lines drawn in Figure 31.

In order to determine the peaks and troughs of the ΔfoF2 variations, the 15-minute ΔfoF2 data in the Austro-Asian sector was plotted with an expanded time scale (about 1 cm graph length per hour time interval). Then the slopes of the ΔfoF2 values were extrapolated graphically. The times corresponding to the slope intersects were then determined to the nearest 0.05 hour and tabulated in Table III. After analyzing the data using the extrapolated peak and trough passage times by the triangulation method below, it was determined that the times of trough passage yielded the more consistent results for different sets of stations. Therefore, only the trough analysis will be discussed.

Least squares analysis of geographic latitude versus trough passage time yielded average apparent equatorward velocities of 718, 543, 378, and 368 m sec^{-1} for the four troughs shown in Figure 31. Manila was not used in the analysis because the troughs were in general not well defined at this station (i.e., peaks where troughs should be).

An alternate explanation of these oscillations in foF2 might be that they are the result of oscillatory electric fields of some sort which cause plasma to flow in and out of a region by $\underline{E}\times\underline{B}$ drifts. However, if the velocities obtained (368 to 718 m sec^{-1}) were $\underline{E}\times\underline{B}$ velocities, the minimum electric fields required to produce

TABLE III

TRAVELLING IONOSPHERIC DISTURBANCES,

2100 UT 2 MAY TO 0930 3 MAY 1976

Geographic Latitude	Station	Peak 1	Peak 2	Peak 3	Peak 4
45.4	Wakkanai	-	1.75	4.30	7.00
39.7	Akita	22.25	2.30	4.40	7.30
35.7	Kokubunji	22.40	(3.00)	4.50	7.60
31.2	Yamagawa	22.40	2.90	5.75	8.00
25.0	Taipei	22.25	2.95	5.90	8.20
16.4	Manila	22.50	1.75	6.30	-

Geographic Latitude	Station	Trough 1	Trough 2	Trough 3	Trough 4	Trough 5
45.4	Wakkanai	0.8	2.90	5.40	8.50	11.70
39.7	Akita	1.1	3.15	5.70	9.00	12.30
35.7	Kokubunji	-	3.25	5.90	9.30	12.70
31.2	Yamagawa	1.4	3.30	6.50	9.70	13.00
25.0	Taipei	1.7	3.70	6.80	-	-
16.4	Manila	-	4.50	7.70	-	-
	V_L (°/hr)	-23.23	-17.58	-12.23	-11.98	10.68
	V (m/sec)	-718	-543	-378	-368	-330
	r	-1.00	-0.96	-0.99	-1.00	-0.99

V_L = velocity (degrees latitude/hour) + = north

V = velocity (meters/second) + = north

r = correlation coefficient to 2 significant digits after decimal.

the drifts would be about 18 to 36 mv m^{-1}. These values are extremely high for the mid-latitude F region, where electric fields are usually on the order of a few mv m^{-1} Therefore, it seems unlikely that the oscillatory foF2 variations observed were the result of $\underline{E}\times\underline{B}$ drifts.

It should be pointed out that even in the absence of thermospheric neutral winds or drifts, several factors can influence gravity wave propagation, and thus the oscillatory foF2 behavior at a given station. These include a) superposition of waves; b) geometry of the gravity wave front; and c) factors which may influence the response of the F-region ionization to the gravity wave passage:

a) Superposition of waves--several gravity waves from separate sources may pass a station in such a way as to constructively or destructively interfere and thus change the wave form (and hence the foF2 behavior) above the station.

b) In theory, a gravity wave in an isotropic atmosphere will spread symmetrically as it travels from a point source. However, the direction of wave propagation can be altered by neutral wind and temperature gradients. The radiation pattern of line source may be concentrated perpendicular to the source axis. Ionization in the F region over stations near the extension of the source axis will therefore be less affected by the

gravity wave passage.

c) Response of the F-region ionization to propagating gravity waves--the most important gravity wave induced electron concentration perturbations occur in the transport term, M, in the electron density continuity equation:

$$\frac{\partial N}{\partial t} = Q - L - M ,$$

where Q is the production rate, L is the loss rate, and N is the electron density (Yeh and Liu, 1974). Transport of plasma to regions of lower or higher loss rate may considerably influence N in such a way that it will not respond in a linear fashion to the gravity wave forcing. Additionally, foF2 is measured at the height of F-region ionization maximum, hmF2, which may vary by 100 km on a typical non-storm day at a given station.

TID horizontal velocity and direction can be determined by the method of triangulation (Davies and Jones, 1972). Several approximations are made in determining the TID velocity and direction of travel by the method of triangulation. Francis (1972) has shown that in an isothermal atmosphere gravity waves may propagate at a roughly constant height above the Earth's surface for thousands of kilometers from a source region. Refraction downward of the wave by the spherically symmetric gravity field can be compensated for by the Earth's

curvature, and the wave travels as if the Earth were a plane surface. Secondly, spherical trigonometry has been replaced by plane trigonometry. The importance of this can be seen from studying Figure 33. In plane geometry,

$$\sin d = \frac{V_H(t_2-t_1)}{A} \quad , \tag{4.2}$$

while the actual relationship on the spherical Earth is

$$\sin d = \frac{\sin[V_H(t_2-t_1)/Re]}{\sin(A/Re)} \quad , \tag{4.3}$$

where V_H is the horizontal trace velocity, $t_1(t_2)$ is the time interval between trough arrival at Wakkanai and Akita (Wakkanai and Yamagawa), A is the great circle distance between Akita and Yamagawa, and Re is the radius of the Earth in the same units. Thus, the arguments of the sines are in radians. For horizontal distances small compared to Re, it can be shown that errors introduced by the plane trigonometry approximation will be small compared to errors introduced by such things as thermospheric drifts and the 15-minute timing rate.

Other approximations introduced are that the foF2 peak is measured at a constant height in the F region, and that thermospheric drifts are absent. Neither of these are strictly true. The approximations are summarized as follows:

1. The TID propagates at a constant height above a plane surface.

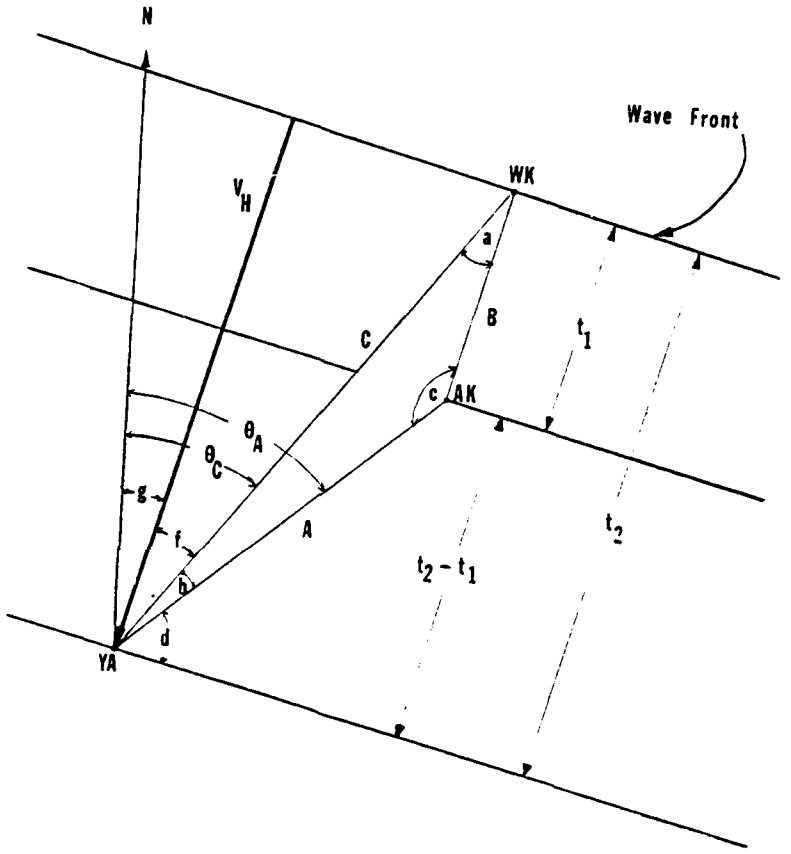

FIGURE 33 Sample geometry for determining horizontal trace velocity from time displacements following the method of Davies and Jones (1972); see text.

2. Plane trigonometry may be used.

3. Timing of trough or crest passage is sufficiently accurate.

4. There are no thermospheric winds.

Then, referring to Figure 33, the azimuth g of the gravity wave horizontal wave vector (direction east of north from which the wave approaches the station), and the horizontal trace velocity V_H can be found as follows:

$$\sin d = V_H(t_2-t_1)/A \quad , \tag{4.4}$$

$$V_H t_2 = c \cos f \quad , \tag{4.5}$$

$$f + d + b = \pi/2 \quad , \tag{4.6}$$

and therefore it can be shown that

$$f = \tan^{-1}\left\{\frac{1}{\sin b}\left[\cos b - \frac{C}{A}\frac{(t_2-t_1)}{t_2}\right]\right\} \quad , \tag{4.7}$$

$$g = \theta wk - f \quad , \tag{4.8}$$

and, rewritting (4.5),

$$V_H = \frac{C \cos f}{t_2} \quad .$$

Trough passage times for several combinations of stations in Table III were used to determine g and V_H by the triangulation method. Sample calculations are tabulated in Table IV.

TABLE IV

SAMPLE AZIMUTHS AND VELOCITIES

FOR TRAVELLING IONOSPHERIC DISTURBANCES 3 MAY 1976*

Trough	t_1 (Hr UT)	t_2 (Hr UT)	f	g (deg)	V_H (m sec^{-1})
1	.3	.6	52.2	-24.1	523
2	.25	.3	64.6	-37.4	530
3	.3	1.1	-20.1	48.3	538
4	.5	1.2	34.4	-6.2	353
5	.6	1.3	45.4	-17.1	277

*Sample azimuth (east of north) and horizontal trace velocity (m sec^{-1}) calculations using the stations Wakkanai, Akita, and Yamagawa for TIDs on 3 May 1976.

The horizontal trace velocities, V_H, determined using the first three trough passages in Table IV (and best defined troughs) were 523, 530, and 538 m sec^{-1}. These values are within the limits reviewed by Richmond and Roble (1979) for large scale TIDs. Additionally, the azimuths indicate pole-to-equator directions of travel. The azimuths and velocities for the troughs in Table IV were used to extrapolate the wave front travel back to possible source regions along great circles. A constant velocity was assumed in each case, and the five TID great circle paths determined from the data in Table IV were plotted on a polar stereographic map (not shown). Times of enhanced aurora (determined from the peaks in AE index, Figure 30) were marked on the great circles by darkened lines as possible TID source regions. The intervals of enhanced aurora were 1800 to 2100 UT on 2 May, 0000 to 0300 UT, and 0600 to 0700 UT on 3 May 1976. No single source rotating with the auroral oval was apparent. This may be due to the widespread extent of the source, or to inaccuracies in the method used to determine the source regions. However, the general source regions do appear to lie in the higher latitude regions.

An unusual peak in foF2 and ΔfoF2 appeared in the Manila data at 0145 UT and in the Taipei and Yamagawa data at 0245 UT on 3 May. The shapes of the three peaks

suggested that they were correlated, and appeared to be progressing poleward. The triangulation method was used to determine the speed and direction of the suspected TID. V_H was found to be 153 m sec^{-1} travelling from a direction of about 140^{o} east of north. If this series of peaks actually corresponds to the passage of a TID, it was therefore either generated in the southern hemispheric auroral zone, or, less likely, perhaps in the equatorial electrojet. A poleward progression of foF2 peaks can also be seen in the data from the Austro-Asian chain of stations at about 0200 UT on 5 August 1972 (Koizumi et al., 1974). It is interesting to note that the maximum change in Dst occurred between 0000 and 0100 UT on 3 May 1976. Alternately, these peaks may be related to the dayside disturbance in the early hours of 3 May discussed in the previous section. It must be pointed out that the series of peaks at about 1000 local time may indeed be a local time effect rather than evidence by the TEC data from Ootacamund, India. The data for 3 May 1976 shows a late morning peak at about 1000 LT (Bouwer et al., 1979).

The TID observations in this section can be summarized as follows:

1. Apparent horizontal TID velocity in the north-south direction ranged from 718 m sec^{-1} to 368 m sec^{-1}. These velocities are on the order of those expected to

be observed associated with long period (2-3 hours) internal gravity waves (see Appendix A).

2. The triangulation method yielded TID actual horizontal trace velocities of 530 m sec^{-1} to 277 m sec^{-1} with directions of travel from the northeast or northwest, suggesting sources in the auroral zone.

3. A possible poleward TID appeared at the stations Manila, Taipei, and Yamagawa. The velocity (153 m sec^{-1}) and direction (from the southeast) suggest the passage of a medium scale TID at these stations.

CHAPTER 5

DISCUSSION AND CONCLUSIONS

5.1 Interpretation of Observations

The general features of the ionospheric disturbance period 30 April to 5 May 1976 may be interpreted in terms of presently available models, or at least theoretical ideas, of the disturbance mechanisms.

As discussed in section 4.2, the period of March to May 1976 occurred at sunspot minimum, and yet solar activity was at times quite enhanced during this interval. Interplanetary regions of higher solar wind bulk speed appeared to co-rotate with the sun and were associated with increases in geomagnetic activity at 27-day intervals in early March, April, and May. Therefore, it must be kept in mind that the 30 April solar flare and subsequent terrestrial response were superimposed on the background recurring phenomena.

The ionospheric response to the 30 April 1976 major solar flare (X-ray onset at 2043 UT) was not unusual (section 3.3). The enhancement in fmin, coincident with the flare, corresponds to increased D-region ionization by X-rays at wavelengths in the 1-10 Å range (Rishbeth and Garriott, 1969, p. 106). The geomagnetic

SFE observed at Boulder and Huancayo suggests E-region ionization by radiation in the 10-170 Å range. The F2 region, where the constituents O and N_2 are ionized by solar radiation in the 170-911 Å range, showed a general lack of response to the solar flare. However, this does not imply that the X-ray and EUV flare spectrum peaked at wavelengths shorter than 170 Å. Most EUV radiation is absorbed in the atmosphere below 200 km (below the F2 peak electron density), therefore the F2 region may not respond directly to enhancements in the EUV spectrum.

The ionospheric storm mechanisms have been outlined in Chapter 2 and are summarized here. The positive phase of ΔfoF2 variations are most likely present at locations where the geomagnetic SSC occurred between 0600 and 1500 LT (Mendillo, 1973). Possible explanations of this initial enhancement of F-region ionization include:

1. Equatorward neutral winds transport plasma up along geomagnetic field lines to a region where the ionization loss rate is lower. The source of these thermospheric winds include Joule heating and Lorentz forces in the dayside auroral zone (Jones and Rishbeth, 1971).

2. Storm-time electric field (in the ionospheric E region) with an eastward component causes an $\underline{E}\times\underline{B}$ plasma drift upward to a region of lower ionization loss rate (Matuura, 1972).

Anderson (1976) suggested that a poleward electric field, centered at 1800 LT, would cause a westward plasma drift, resulting in an ionization enhancement in the local afternoon.

The negative phase of the ionospheric storm is due mainly to increases in the F-region ionization loss rate. The dominant positive ion in the F region is O^+, since molecular ions, O_2^+ and N_2^+, are rapidly lost by dissociative recombinations of the form:

$$N_2^+ + e^- \rightarrow N + N \quad . \tag{5.1}$$

The loss of O^+ (and e^-) can be accomplished by rapid reactions of the sort

$$O^+ + N_2 \rightarrow NO^+ + N \quad , \tag{5.2}$$

then

$$e^- + NO^+ \rightarrow N + O \quad . \tag{ .3}$$

Therefore, higher loss rates may be caused by the increase in neutral constituents (Ratcliffe, 1972, p. 43). The ion-atom interchange process is thought to dominate the F-region negative ΔfoF2 storm phase. The storm circulation transports composition changes equatorward. This increases the N_2/O ratio upon which the O^+ loss rate depends (Davies, 1974; Rishbeth, 1975). The sharp onset of the negative phase of the ionospheric storm at mid-latitudes may be caused by the equatorward

propagation of a "front" of air mass with increased neutral constituents (Davies, 1974), or due to the westward drift proposed by Anderson (1976).

Recent computer simulation studies of worldwide ionospheric electric fields and currents produced by field-aligned currents have been made by Kamide and Matsushita (1979a, 1979b). They numerically solved the steady state equation for current conservation using various combinations of anisotropic electric conductivities and exponentially distributed downward and upward field-aligned currents in the auroral region. Among their results, they found that even a slight enhancement in conductivity in the night-side auroral zone results in a large modification of the global electric field pattern. Using conductivities and field-aligned current values characteristic of those observed during intense substorms, the numerical analysis by Kamide and Matsushita (1976) produced the electric potential pattern shown in Figure 34. Northward (eastward) electric fields appear in the afternoon (morning) dayside sectors even at mid-latitudes ($\underline{E} = -\underline{\nabla}\Phi$). The resulting $\underline{E}\times\underline{B}$ drifts from the dayside potential field would be westward in the afternoon and upwards in the morning sectors.

This model provides support to the suggestion that electric fields may appear at mid and low latitudes during substorms. Electrodynamic ($\underline{E}\times\underline{B}$) drifts set up

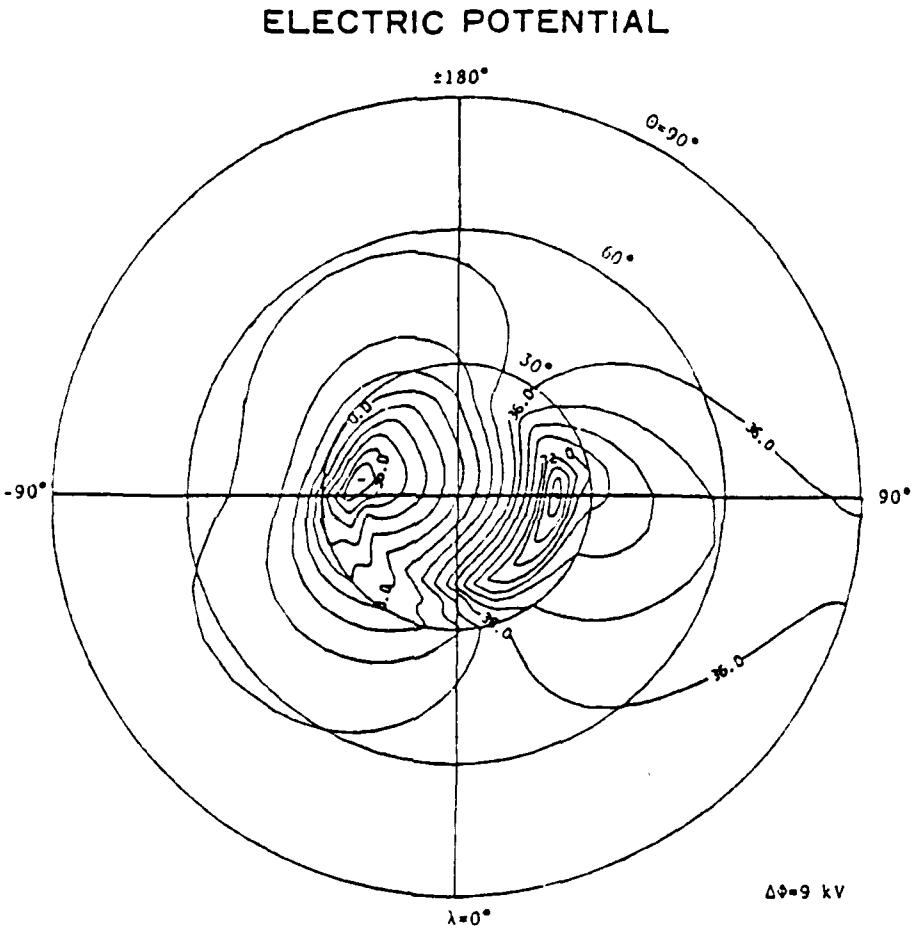

FIGURE 34 Electric potential due to field-aligned current system, obtained using the computer simulation analysis by Kamide and Matsushita (1979b). Equi-potential lines are drawn for the northern hemisphere at 9 kV intervals. Theta corresponds to co-latitude, while λ is east longitude relative to local midnight, i.e., $\lambda = 180^{o}$ corresponds to local noon.

by the storm $\underline{E}$ field pattern can cause accumulation of plasma in regions of lower or higher loss rates. In this manner large variations in ionization may occur during intense substorm periods, even at middle and low latitudes.

The initial enhancement over Europe on the afternoon of 2 May could have resulted from the lifting of ionospheric plasma by either (1) of (2) above. However, the simultaneous positive ΔfoF2 response (Figure 27) suggests that method (2) dominated. A front of enhanced neutral constituent concentration, transported equatorward by the neutral wind, would then account for the negative phase.

The geomagnetic substorms on 2 May 1976 (see the AE index in Figure 30) may have been sufficiently intense to initiate the negative storm mechanism before the SSC at 1830 UT on 2 May 1976. This would account for the general absence of the ionospheric storm positive phase following the SSC at high and mid-latitudes, except at Maui and Raratonga. Air masses with increased ionization loss rates may not have had time to reach these lower mid-latitude stations by the time of SSC. Davies (1974) gives equatorward speeds of the negative phase "front" to be 50 to 150 m sec^{-1} (1.5^{o}/hr to 4.5^{o}/hr) based on Matsushita's (1959) analysis. Additionally, these pacific sector stations meet Mendillo's (1973) criteria

for the onset of the positive storm phase (i.e., SSC between 0600-1500 LT).

The negative phase of the main ionospheric storm would then be explained by the large substorm activity in high latitudes following the SSC, using the equatorward thermospheric flow model.

The afternoon enhancement and rapid decrease in ΔfoF2 after sunset at higher and mid-latitude stations during the 2-5 May 1976 storm followed the general beahvior observed in previous ionospheric storm studies. Anderson's (1976) model could account for this behavior where an equatorward neutral wind is coupled with a westward drift of ionization.

The unusually large and sudden F-region disturbance on the sunlit hemisphere shortly after 0000 UT on 3 May 1976 may have been associated with the intense substorm activity at this time, shown by the AE index in Figure 30 and low latitude magnetograms in Figure 21. Referring to Kamide and Matsushita's simulation, it is plausible that electric fields in mid and low latitudes were set up by the intense substorm between 0000 and 0300 UT on 3 May 1976. These $\underline{E}$ fields may have been responsible for the widespread F-region disturbances observed at that time. An explanation of this sort is easier to visualize than one requiring the mapping down along field lines of storm time magnetospheric electric fields. In

the field-aligned current model, the electric fields necessary to initiate plasma drifts are already present in the ionosphere (in general, at E-region altitudes).

The question may be asked, Can the electric fields generated by Kamide and Matsushita's model produce the observed ionization during this period? The peak enhancement in NmF2 over Boulder at 0100 UT 3 May 1976 (Figure 25) was about 155%, determined from the relationships:

$$NmF2 = k(foF2)^2 , \qquad (3.2)$$

$$\Delta NmF2\ (\%) = \frac{NmF2 - NmF2\ (median)}{NmF2\ (median)} , \qquad (5.4)$$

or

$$\Delta NmF2\ (\%) = \left[\frac{foF2}{foF2\ (median)}\right]^2 - 1 , \qquad (5.5)$$

where foF2 = 8.3 MHz, foF2 (median) = 5.2 MHz at this time. (These relationships were used instead of the approximate formula 3.4 because the deviation of foF2 from the median was rather large--about 60%.) A rough value of the ionosphere electric field over Boulder at this time (1800 LT) was obtained using the poleward electric potential at Boulder's latitude in Figure 34, and the approximate relationship

$$E = \frac{\Delta\Phi}{\Delta L} , \qquad (5.6)$$

where $\Delta\Phi$ is the electric potential between contours (9×10^6 mV) and ΔL is the distance between lines (about

$7.2^{o} \approx 8\times10^{5}$ m). The poleward electric field of 11 mV m^{-1} determined in this way (assumed perpendicular to the geomagnetic field line) corresponds to a westward $\underline{E}\times\underline{B}$ plasma drift of about 200 m sec^{-1}. Evans (1973) observed westward drifts of 200 m sec^{-1} in the F region over Millstone Hill (55^{o} N geomagnetic) at 1800 LT in May 1969 during a magnetically disturbed day (maximum Kp = 8). Anderson (1978) used values characteristic of this data and observed meridional winds and solved the time-dependent O^{+} continuity equation to evaluate the response of the F-region to east-west plasma drifts produced by poleward electric fields at 55^{o}N latitude (Earth-centered dipole approximation). Enhancements in NmF2 at 1800 LT reached about 200% using Anderson's model for an equatorward wing of 100 m sec^{-1} and a poleward $\underline{E}$ field of 9 mV m^{-1}. Anderson concludes that in this model the westward plasma drift, when combined with the equatorward neutral wind, causes an enhancement in NmF2 at sunset which would not occur if the ionosphere were co-rotating with the Earth. Therefore, it appears that electric fields at mid-latitudes can produce the ionization changes observed during intense substorms.

The roughly 2.5-hour periods of ΔfoF2 oscillations in the Japanese chain was interpreted here as indicating the passage of large-scale travelling ionospheric disturbances. Attempts to trace the TIDs back to source

regions have been only partially successful due to many complicating factors mentioned in section 4.5. The sources appear to lie in high latitudes, giving support to the models of gravity wave generation by substorm phenomena in the auroral belt. A theoretical investigation of internal gravity waves by Richmond (1978a) suggests that pressure forces due to Joule heating dominate over Lorentz forces in driving gravity waves observed several thousand km from auroral source regions. Richmond (1978a) pointed out that the efficiency of wave energy production (total wave energy generated/total energy input) depends both upon the strength of the electric field and upon the geometry of the source. In a numerical simulation using an exponentially varying pole-centered heat source, Richmond found that a total energy input of 1.53×10^{13} J generated a total wave energy of 3.3×10^{10} J. Similar models require energy inputs of about 10^{15}-10^{16} J to duplicate observed gravity wave features observed at mid-latitudes (see for example: Roble et al., 1978; Richmond and Roble, 1979). See also Appendix B. It is not possible to determine whether one single impulse generated the series of TIDs, or whether they were due to energy input during the series of substorms. Oscillatory foF2 behavior following impulsive events, such as nuclear explosions, have been observed (Row, 1967). Observations and gravity wave

theory indicate that the period of TID oscillations increase with distance from the source (Francis, 1975; Richmond 1978). In the analysis of section 4.5, it was found that the equatorward TID velocities, determined by the trough passage times, decreased at each oscillation. This could also be interpreted as an increase in period of foF2 oscillations with increased distance from the polar region, i.e., the time between troughs increases equatorward.

One interpretation of the peaks in ΔfoF2 at about 0900-1100 LT (0000-0200 UT) on 3 May observed over Manila, Taipei, and Yamagawa (Figure 32), was that they indicated the passage of poleward travelling TIDs, as discussed in section 4.5. The direction (toward the pole) and velocity (less than the lower atmosphere sound speed) argue against these peaks representing a large scale TID. Some substorm associated electric field enhancement could cause upward and westward plasma drifts reaching maximum in the late morning associated with substorm maximum intensity (Figure 30). The late morning ΔfoF2 peak was probably not due to diffusion of plasma from the geomagnetically conjugate point along the field lines when that point experience enhanced ionization after its later sunrise. This is because foF2 in the Japanese chain of stations remained above the foF2 in northern Australia (the conjugate latitude).

Thus, the gradient in plasma density would have prevented diffusion from the winter (southern) to summer (northern) hemisphere.

Takenoshita et al. (1974) found equatorward propagating TIDs over Japan during the August 1972 events and what they interpreted as east-west travelling TIDs near sunrise and sunset. A similar interpretation of the post-sunrise and 1000 LT foF2 peaks noted in this paper is that the peaks are also E-W travelling TIDs. Francis (1975) reported that one source of these TIDs might be gravity waves launched by the supersonic velocity of the sunrise-sunset terminator.

Similarities are found between the ionospheric storm following the 1830 UT 2 May 1978 SSC and that following the 2054 UT 4 August 1972 SSC. Paul et al. (1977) analyzed the 4-5 August 1972 storm events in the Asia-Australia-Pacific sector of the globe using 35 middle and low latitude ionospheric stations and 7 geomagnetic stations. Matsushita (1976) reviewed the worldwide ionospheric and thermospheric response to solar events during the first half of August 1972 and discussed the findings in terms of current storm models and theories. Both SSCs occurred on days about half way between equinox and summer in the northern hemisphere when the solar declination angle was about $+15^{o}$.

The subsolar point at the time of SSC in each case

was in the western N-S American sector. The similarities in ionospheric behavior include:

1. The large main phase decrease in ΔfoF2 at Maui and the absence of the decrease at Raratonga.

2. A large peak in ΔfoF2 at about 1000 LT (0100 UT) in the Japanese sector on the first storm day. (Koizumi et al., 1974, and Figure 32 in this work.)

3. Roughly 2.5-hour oscillations in the Japanese sector (Koizumi et al., 1974).

The similarities in F-region behavior during the two storms at different periods in the solar cycle suggest that the same mechanisms contribute to ionospheric storm behavior regardless of the level of solar activity.

The Maui-Raratonga ΔfoF2 behavior during the present storm showed close correlation during the early period of the ionospheric storm. However, the large decrease in ΔfoF2 ($\sim$5 MHz) on 4 May 1976 at Maui was absent at Raratonga, Maui's geomagnetic conjugate point. In other words, the actual foF2 values at both stations were roughly the same during Maui's large negative ΔfoF2 phase. This indicates plasma flow along the geomagnetic field lines from the summer (Maui) to winter (Raratonga) hemisphere. Again, Matsushita (1977) found a similar result during the main phase of the 4-5 August 1972 storm period. An alternate interpretation would be that excess plasma in the summer hemisphere is removed by the neutral

constituents transported equatorward during the storm.

5.2 Conclusions

The study period 30 April to 5 May 1976 provided a unique opportunity to investigate the ionospheric response to solar disturbances during solar sunspot minimum. As discussed in section 5.1, current theories of ionospheric storm mechanisms provide plausible explanations of the general features of the positive and negative phase of the ΔfoF2 variations observed. Also, substorm occurrence may cause local ionospheric disturbances prior to geomagnetic SSC. Recent numerical simulation studies of field-aligned-current electric fields and currents, such as those by Kamide and Matsushita (1979a, 1979b), suggest that auroral electric fields may extent to middle and low latitudes during intense substorms. However, steady-state computer models say nothing of the time dependency of the electric field.

Therefore, a plausible mechanism exists for the generation of ionospheric electric fields necessary to explain observed drifts and plasma density variations, without requiring the mapping down of magnetospheric electric fields to low latitudes.

Large scale travelling ionospheric disturbances are difficult to analyze with the limited number of stations and the 15-minute sampling rate provided by

conventional ionospheric observatories.

True density variations with height of the ionospheric plasma and electric field and plasma drift observations during ionospheric disturbances are required for the confirmation of the proposed storm mechanisms.

Additional ionospheric storm studies need to be conducted to determine the source of the post-dawn maximum of foF2 and larger peak 2-3 hours later observed in the Eurasian sector. These enhancements appear to be a local time effect and occur on the first morning (at least) following the SSC.

REFERENCES

AFGL Special Report No. 209, Contributed Papers to the Study of Travelling Interplanetary Phenomena/1977 (eds., M. A. Shea, D. F. Smart, and S. T. Su), 1977.

Akasofu, S.-I., Magnetospheric substorms, EOS Trans. AGU, 59, 68-73, 1978.

Akasofu, S.-I., and S. Chapman, Solar Terrestrial Physics, Clarendon, Oxford, 1972.

Akasofu, S.-I., and L. J. Lanzerotti, The Earth's magnetosphere, Phys. Today, 21-12, 28-35, 1975.

Anderson, D. N., Modeling the midlatitude F-region ionospheric storm using east-west drift and a meridional wind, Planet. Space Sci., 24, 69-77, 1976.

Appleton, E. V., and L. J. Ingram, Magnetic storms and upper-atmospheric ionization, Nature, 136, 548-549, 1935.

Atkinson, G., A theory of polar substorms, J. Geophys. Res., 71, 5157-5164, 1966.

Badillo, V. L., Comparison of low latitude magnetograms of storms during 20 March - 3 May 1976, WDC-A for STP, Rep. UAG-61, 281, 1977.

Bartels, J., Terrestrial-magnetic activity and its relations to solar phenomena, Terr. Magnatmos. Elect., 37, 1-52, 1932.

Bouwer, S. D., K. Davies, R. F. Donnelley, R. G. Rastogi, M. R. Deshpande, H. Chandra, and G. Sethia, ATS-6 radio beacon electron content measurements at Ootacamund, India, from October 1975 to July 1976, WDC-A for STP, Rep. UAG, to be published, 1979.

Burlaga, L. F., and K. W. Ogilvie, Causes of sudden commencements and sudden impulses, J. Geophys. Res., 74, 2815-2825, 1969.

Carrington, R. C. (no article title), Monthly Notices Roy. Astron. Soc., 29, 13, 1859.

Castelli, J. P., and W. R. Barron, Highlights of solar radio data 20 March - 5 May 1976, WDC-A for STP Rep. UAG-61, 39-47, 1977.

Chimonas, G., The equatorial electrojet as a source of long period travelling ionospehric disturbances, Planet. Space Sci., 18, 583-589, 1970.

Davies, K., Studies of ionospheric storms using a simple model, J. Geophys. Res., 79, 605-613, 1974.

Davies, K. National Buerau of Standards Monograph 80: Ionospheric radio propagation, U.S. Government Printing Office, 1965.

Davies, K., Recent progress in satellite radio beacon studies with particular emphasis on the ATS6 radio beam experiment, Ms. No. IPA-78-16, 1978.

Davies, K., and D. M. Baker, Ionospheric effects observed around the time of the Alaskan earthquake of March 28, 1964, J. Geophys. Res., 70, 2251-2253, 1965.

Davies, K., and J. E. Jones, NOAA Professional Paper 6: Ionospheric disturbances produced by severe thunderstorms, U.S. Government Printing Office, 1972.

Davis, T. N., and M. Sugiura, Auroral electrojet activity index AE and its universal time variations, J. Geophys. Res., 71, 785-801, 1966.

Dieminger, W., and H. Kohl, Effects of nuclear explosions on the ionosphere, Nature, 193, 953-964, 1962.

Donnelly, R. F., The solar flare radiations responsible for sudden frequency deviations, J. Geophys. Res., 72, 5247-5256, 1967.

Dodson, H. W., and R. R. Hedeman, Overall evaluation of major centers of activity on the solar disk, 20 March - 5 May 1976, WDC-A for STP Rep. UAG-61, 10-17, 1977.

Draitsky, V. M., V. A. Ulyev, and A. V. Shirochkov, Polar cap absorption event of 30 April - 3 May 1976 by the riometer data at the Soviet arctic and antarctic stations, WDC-A for STP Rep. UAG-61, 248-251, 1977.

Dungey, J. W., Interplanetary magnetic field and the auroral zones, Phys. Rev. Letters, 6, 47-48, 1961.

Egeland, A., O. Holter, and A. Omholt, editors, Cosmical Geophys., Universitetsforlaget, Oslo, Norway, 1973.

Evans, J. V., Millstone Hill incoherent scatter observations, WDC-A for STP Rep. UAG-28, 497-501, 1973.

Francis, S. H., Propagation of internal acoustic-gravity waves around a spherical earth, J. Geophys. Res., 77, 4221-4226, 1972.

Francis, S. H., Global propagation of atmospheric gravity waves: a review, J. Atmos. Terr. Phys., 37, 1011-1054, 1975.

Hafstad, L. R., and M. A. Tube, Note on Kennelly-Heaviside Layer observations during a magnetic storm, Terrest. Mag. Atmospheric Elect., 34, 39-44, 1929.

Hartmann, G. K., W. Degenhardt, and R. Leitinger, Comparitive study of ATS-6 data from Lindau-Harz and from Graz/Austria, The Geophysical Uses of Satellite Beacon Observations (ed., M. Mendillo), Boston, Boston University, p. 219, 1976.

Hines, C. O., Internal atmospheric gravity waves at ionospheric heights, Can. J. Phys., 38, 1441-1481, 1960.

Huang, Y.-N., Ionospheric variations at Taiwan associated with geomagnetic storms of 26 March, 1 April, and 2 May 1976, WDC-A for STP Rep. UAG-61, 228-231, 1977.

IAGA Bulletin No. 32g (ed. D. van Sabben), Geomagnetic Data 1977, IUGG Publications Office, 39 Ter Rue Gay, Lussac, Paris, 1977.

Ichinose, T., and T. Oagawa, HF Doppler observations associated with McMath regions 14143 and 14179, WDC-A for STP Rep. UAG-61, 245-256, 1977.

Jakowski, N., and B. Lazo, Significant events in TEC measurements between 20 March and 5 May 1976, WDC-A for STP Rep. UAG-61, 232-235, 1977.

Jones, K. L., and H. Rishbeth, The origin of storm increases of mid-latitude F-layer electron concentration, J. Atmos. Terr. Physics, 33, 391-401, 1971.

Kamide, Y., and S. Matsushita, Simulation studies of ionospheric electric fields and currents in relation to field-aligned currents: 1. Quiet periods, J. Geophys. Res., in press, 1979a.

Kamide, Y., and S. Matsushita, Simulation studies of ionospheric electric fields and currents: 2. Substorms, J. Geophys. Res., in press, 1979b.

Knecht, R. W., and K. Davies, Solar flare effect in the F region of the ionosphere, Nature, 190, 797-789, 1961.

Koizumi, T., H. Ohymaa, S. Hiidome, and Y. Echizenya, General features of ionospheric disturbances that appeared in vertical sounding, J. Radio Res. Lab., 21, 371-378, 1974.

Kopp, R. A., and T. E. Holzer, Dynamics of coronal hole regions, Solar Phys., 49, 43-56, 1976.

Krieger, A. S., A. F. Timothy, and E. C. Roelof, A coronal hole and its identification as the source of a high velocity solar wind stream, Solar Phys., 29, 505-525, 1973.

Leonard, R. S., and P. A. Barnes, Observation of ionospheric disturbances following the Alaskan earthquake, J. Geophys. Res., 70, 1250-1253, 1965.

Levine, R. H., M. D. Altschuler, and J. W. Harvey, Solar sources of the interplanetary magnetic field and solar wind, J. Geophys. Res., 82, 1061-1065, 1977.

Martyn, D. F., Atmospheric tides in the ionosphere. I. Solar tides in the F2 region, Proc. Roy. Soc., A189, 241-260, 1947.

Martyn, D. F., The morphology of the ionospheric variations associated with magnetic disturbances. I. Variations at moderately low latitudes, Proc. Roy. Soc., A218, 1-18, 1953.

Martyn, D. F., The normal F region of the ionosphere, Proc. Inst. Radio Engrs., 47, 147-155, 1959.

Matsushita, S., A study of the morphology of ionospheric storms, J. Geophys. Res., 64, 305-321, 1959.

Matsushita, S., On geomagnetic sudden commencements, sudden impulses, and storm durations, J. Geophys. Res., 65, 3753-3777, 1962.

Matsushita, S., Geomagnetic storms and related phenomena, Research in Geophysics, editor, H. Odishaw, Boston, M.I.T., 1965.

Matsushita, S., IMF polarity effects on the Sq current focus location, J. Geophys. Res., 80, 4751-4754 19 .

Matsushita, S., Ionospheric and thermospheric responses during August 1972 storms - a review, Space Sci. Rev., 19, 713-737, 1976.

Matsushita, S., IMFP effects on the equatorial geomagnetic field and ionosphere - a review, J. Atmos. Terr. Phys., 39, 1207-1215, 1977.

Matsushita, S., and B. B. Balsley, A question of DP-2, Planet. Space Sci., 20, 1259-12-7, 1972.

Matsushita, S., and J. D. Tarpley, Effects of dynamo-region electric fields on the magnetosphere, J. Geophys. Res., 75, 5433-5443, 1970.

Matuura, N., Theoretical models of ionopsheric storms, Space Sci. Rev., 13, 124-189, 1972.

Maxwell, A., Solar radio burst of spectral Type II recorded at Fort Davis, Texas, during the period 20 March - 2 May 1976, WDC-A for STP Rep. UAG-61, 79-99, 1977.

Mendillo, M., A study of the relationship between geomagnetic storms and ionospheric distrubances at mid-latitudes, Planet. Space Sci., 21, 349-358, 1973.

Mendillo, M., and J. V. Evans, Incoherent scatter observations of the ionospheric response to a large solar flare, Radio Sci., 9, 197-203, 1974.

Mendillo, M., J. A. Klobuchar, R. B. Fritz, A. V. daRosa, L. Kersley, K. C. Yeh, B. J. Flaherty, S. Rangaswamy P. E. Schimd, J. V. Evans, J. P. Schödel, D. A.

D. A. Matsoukas, J. R. Koster, A. R. Webster, and P. Chin, Behavior of the ionospheric F region during the great solar flare of August 7, 1972, J. Geophys. Res., 79, 665-672, 1974.

Nolte, J. T., A. S. Krieger, A. F. Timothy, R. E. Gold, E. C. Roelof, G. Viana, A. J. Lazarus, J. D. Sullivan, and P. S. McIntosh, Coronal holes as sources of solar wind, Solar Phys., 46, 303, 1976.

Park, C. G., Westward electric fields as the cause of nighttime enhancements in electron concentrations in midlatitude F region, J. Geophys. Res., 76, 4560-4568, 1971.

Paul, M. P., S. Matsushita, and A. D. Richmond, Ionospheric storm of 4-5 August 1972 in the Asia-Austrialia-Pacific sector, J. Atmos. Terr. Phys., 39, 43-50, 1977.

Piddington, J. H., The closed model of the Earth's magnetosphere, J. Geophys. Res., 84, 93-100, 1979.

Rastogi, R. G., and H. Chandra, Interplanetary magnetic field and the equatorial ionosphere, J. Atmos. Terr. Phys., 36, 377-379, 1974.

Rastogi, R. G., and V. L. Patel, Effect of interplanetary magnetic field on the ionospheric over the magnetic equator, Proc. Indian Acad. Sci., 82, 121-141, 1975.

Ratcliffe, J. A., An Introduction to the Ionosphere and Magnetosphere, Cambridge University Press, London, 1972.

Richmond, A. D., Equatorial electrojet - I. Development of a model including winds and instabilities, J. Atmos. Terr. Phys., 35, 1083-1103, 1973.

Richmond, A. D., Equatorial electrojet - II. Use of the model to study the equatorial ionosphere, J. Atmos. Terr. Phys., 35, 1105-1118, 1973.

Richmond, A. D., The nature of gravity wave ducting in the thermosphere, J. Geophys. Res., 83, 1385-1389, 1978a.

Richmond, A. D., Gravity wave generation, propagation, and dissipation in the thermosphere, J. Geophys. Res., 83, 4131-4145, 1978b.

Richmond, A. D., Thermospheric heating in a magnetic storm, J. Geophys. Res., submitted, 1978c.

Richmond, A. D., and S. Matsushita, Thermospheric response to a magnetic substorm, J. Geophys. Res., 80, 2830-2849, 1975.

Richmond, A. D., S. Matsushita, and J. D. Trapley, On the production mechanism of electric currents and fields in the ionosphere, J. Geophys. Res., 81, 547-555, 1976.

Richmond, A. D., and R. G. Roble, Dynamic Effects of aurora-generated gravity waves in the midlatitude ionosphere, J. Atmos. Terr. Phys., in press, 1979.

Rishbeth, H., F-region storms and thermospheric circulation, J. Atmos. Terr. Phys., 37, 1055-1065, 1975.

Rishbeth, H., and O. K. Garriott, International Geophysics Series, Vol. 14: Introduction to Ionospheric Physics, New York, Academic Press, 1969.

Row, R. V., Acoustic-gravity waves in the upper atmosphere due to a nuclear detonation and an earthquake, J. Geophys. Res., 72, 1599-1610, 1967.

Rush, C. M., and A. D. Richmond, The relationship between the structure of the equatorial anomaly and the strength of the equatorial elecrojet, J. Atmos. Terr. Phys., 35, 1171-1180, 1973.

Schindler, K., A theory of the substorm mechanisms, J. Geophys. Res., 79, 2803-2810, 1974.

Schwenn, R., H. Rosenbauer, and K. H. Muhlauser, The Solar wind during STIP II interval: Stream structures, boundaries, shocks and other features as observed by the plasma instruments on Helios-1 and Helios-2, AFGL TR-77-309, ST 309, 351-361, 1977.

SGD-1976, Solar-Geophysical Data, U.S. Department of Commerce, Boulder, Colorado, USA, 80303, 1976.

Shea, M. A., Overview of solar-terrestrial physics phenomena for the retrospective world interval of 20 March - 5 May 1976, WDC-A for STP Rep. UAG-61, 1-9, 1977.

Speiser, T. W., Auroral particles accelerated in the geomagnetic tail, Aurora and Airglow, Reinhold, New York, 491-498, 1967.

Svestka, Z., Geophysics and Astrophysics Monographs, Vol. 8: Solar Flares, D. Reidel Pub. Co., Dordrecht-Holland/Boston, 1976.

Takenoshita, Y., Y. Echizenya, T. Koizumi, and H. Ohyama, Traveling ionospheric disturbances in F-region during the first half of August, 1972, J. Radio Res. Lab., 21, 385-397, 1974.

Turtle, J. P., J. E. Rusmussen, and E. A. Lewis, Riometer, magnetometer, and VLF ionosonde data from the polar cap, 21 March - 8 May 1976, WDC-A for STP Rep. UAG-61, 252-269, 1977.

UAG-10, Report, Atlas of Ionograms, WDC-A for Solar Terr. Phys., NOAA, Boulder, Colorado (Ed., A. H. Shapley), 1970.

UAG-23, Report, U.R.S.I. Handbook of Ionogram Interpretation and Reduction, WDC-A for Solar Terr. Phys., NOAA, Boulder, Colorado (e.g., W. R. Piggott and K. Rawer), 1972.

UAG-23 (revision), U.R.S.I. Handbook of Ionogram Interpretation and Reduction--Revision of Chapters 1-4, WDC-A for Solar Terr. Phys, NOAA, Boulder, Colorado (ed., W. R. Piggott and K. Rawer), 1978.

UAG-28, Report, Collected data reports on August 1972 Solar-terrestrial events, WDC-A for Solar Terr. Phys., NOAA, Boulder, Colorado (ed., H. E. Coffey), 1973.

UAG-61, Report, Collected Data Reports from STIP Interval II, 20 March - 5 May 1976 WDC-A for Solar Terr. Phys., NOAA, Boulder, Colorado (ed., H. E. Coffey and J. A. McKinnon), 1977.

Yeh, K. D., and C. H. Liu, Acoustic-gravity waves in the upper atmosphere, Rev. Geophys. Space Sci., 12, 193-216, 1974.

APPENDIX A

INTERNAL GRAVITY WAVES

In a non-rotating, plane stratified isothermal atmosphere, the linearized equations of motion reduce to

$$\rho \frac{\partial u}{\partial t} = - \frac{\partial p}{\partial x} , \tag{A.1}$$

$$\rho \frac{\partial v}{\partial t} = - \frac{\partial p}{\partial y} , \tag{A.2}$$

$$\rho \frac{\partial w}{\partial t} = - \frac{\partial p}{\partial z} - \rho g , \tag{A.3}$$

where ρ = atmospheric density, g = gravitational acceleration (assumed constant), p = pressure, and u,v,w = velocities in the x,y,z directions, z assumed positive upwards (Akasofu and Chapman, 1972).

Plane wave solutions are sought of the form:

$$\exp(z/2H) \; \exp i(\omega t - k_x x - k_y y - K_z z) , \tag{A.4}$$

which gives the dispersion relationship

$$\omega^4 = \omega^2 c^2 (k_H^2 + k_z^2) + (\gamma - 1) g^2 k_H^2 - \frac{\gamma^2 g^2 \omega^2}{4c^2} = 0 \tag{A.5}$$

where $c = \gamma g H$ = sound speed, $H = kT/mg$ = scale height $k_H = (k_x^2 + k_y^2)^{\frac{1}{2}}$ = horizontal wave number, $K_z = k_z + i/2H$, and γ is the ratio of specific heats.

Two types of waves can propagate in this situation:

acoustic waves, $\omega > \omega_a \equiv \gamma_g/2c$; (A.6)

internal gravity waves, $\omega < \omega_g \equiv (\gamma-1)^{\frac{1}{2}}g/c$. (A.7)

Davies and Jones (1972) give the refractive index, μ, of acoustic-gravity waves in an isothermal atmosphere:

$$\mu^2 = \frac{c^2}{v^2} = \frac{1-x}{1-y^2\sin^2\phi} \quad , \tag{A.8}$$

where $x = (\omega_a/\omega)^2$, $y = \omega_g/\omega$, and ϕ is the angle of propagation with respect to the vertical.

For an internal gravity wave propagating with angle ϕ to the vertical, and with period on the order of 2-3 hours, the apparent horizontal velocity, v_H, is related to the actual phase velocity,

$$v = \frac{\omega}{k} = V_H\sin\phi \quad ,$$

and $\omega << \omega_a, \omega_g$ at F-region altitudes (where $T_a \lesssim T_g \approx 5$ minutes). Equation (A.8) then reduces to

$$\frac{c^2}{V_H^2} \approx \frac{\omega_a^2}{\omega_g^2} \quad ,$$

or,

$$V_H \approx c\,\frac{\omega_a}{\omega_g} = \frac{c\,\gamma}{2(\gamma-1)^{\frac{1}{2}}} \quad , \tag{A.9}$$

It is important to note that V_H is independent of ζ in this low frequency approximation, and that the wave is non-dispersive. At F-region altitudes, where monatomic oxygen is the dominant neutral constituent, $\gamma \approx 1.6$, and

$$V_H \approx 1.1\ c \approx 700\ m\ sec^{-1}.$$

Therefore, we would expect the apparent horizontal velocity of internal gravity waves, with periods of 2-3 hours, to be independent of period and ϕ, and to propagate at about the local sound velocity.

APPENDIX B

JOULE DISSIPATION AS A HEAT SOURCE IN THE AURORAL ZONE

Ignoring gravity, pressure-gradient forces, and electron-ion collisions, the equation of motion for any charged particle in electric fields, $\underline{E}$, and magnetic fields, $\underline{B}$, is:

$$m \frac{d\underline{V}}{dt} = e(\underline{E}+\underline{V}\times\underline{B}) - m\nu(\underline{V}-\underline{U}) \quad ,$$

where m = mass of particle, e = charge, $\underline{V}$ - particle velocity, $\underline{U}$ = neutral air velocity, and ν = an effective neutral-electron collision frequency. The electric field $\underline{E}$ can be separated into components parallel and perpendicular to the magnetic field, $\underline{E}_{||}$ and $\underline{E}_{\perp}$. Ohm's law, relating current density $\underline{j}$ to the fields, may then be written

$$\underline{j} = \sigma_0\underline{E}_{||} + \sigma_1\underline{E}_{\perp} + \sigma_2 \frac{\underline{B}\times\underline{E}_{\perp}}{B} \quad ,$$

where, summing over all charged particles in species r, the conductivites are given by:

$$\sigma_0 = \frac{1}{B} \sum_r \frac{n_r\omega_r}{\nu_r} e_r \qquad \text{direct} \quad ,$$

$$\sigma_1 = \frac{1}{B} \sum_r \frac{n_r \nu_r \omega_r}{\omega_r^2 + \nu_r^2} e_r \qquad \text{Pedersen}$$

$$\sigma_2 = -\frac{1}{B} \sum_r \frac{n_r \omega_r^2}{\nu_r^2 + \omega_r^2} e_r \qquad \text{Hall} \quad ,$$

where n_r = number density, ω_r = gyrofrequency, and ν_r is the collision frequency of charged particle of species r with the neutrals (Matsushita and Campbell, 1968, p. 381).

The rate of heating by Joule dissipation is given by

$$Q = \underline{j} \cdot \underline{E} \ .$$

If the magnetic field lines may be considered equipotentials ($E_{||} = 0$) and noting that $j \cdot E = 0$ for the Hall current, then

$$Q = j_p^2 / \sigma_1 \ ,$$

where σ_1 is the Pedersen conductivity above and j_p is the Pedersen contribution to the current.